An elastance-based control scheme for a heart valve tester

van Gerven, L.H.M.

Award date:
2005

An elastance-based control scheme for a heart valve tester

Master's thesis
by L.H.M. van Gerven
DCT 2005.14, BMTE 05.10

Engineering Thesis Committee:

prof.dr.ir. M. Steinbuch (CST)
dr.ir. M.C.M. Rutten (BMT)
dr.ir. M.J.G. van de Molengraft (CST)
dr.ir. P.H.M. Bovendeerd (BMT)
dr.ir. R.H.B. Fey (DCT)

Eindhoven University of Technology (TUE)
Department of Mechanical Engineering
Control Systems Technology Group

Eindhoven, February 2005

Contents

1 Introduction 5

2 Materials and concepts 6

2.1 Outline of the approach 6

2.2 Mathematical model of the heart valve tester 7

2.2.1 Hemodynamic preload and afterload 7

2.2.2 Cardiac valves 9

2.2.3 Pump and piston 9

2.2.4 The time-varying elastance model 10

2.2.5 Settings of the model parameters 11

2.3 Control concept 12

2.3.1 Servo controller 13

2.3.2 Stability 14

2.4 Implementation of the control concept 15

2.4.1 Data acquisition 15

2.4.2 Initialization 15

2.4.3 Signal conditioning 16

3 Results 17

4 Discussion 19

5 Conclusion 21

A Anatomy and physiology of the heart 23

B Determination of pump compliance C_p 24

C Concept with feedback of pump pressure p_p 24

D Stability analysis 28

D.1 Stability of concept with feedback of piston position x_1 30

D.2 Stability of concept with feedback of pump pressure p_p 31

E FRF and servo controller design for the heart valve tester 32

F Measuring frequency response functions 35

F.1 Direct method 36

F.2 Sensitivity method 37

G Introduction to controller design 38

G.1 Closed loop stability 39

G.2 Disturbance rejection and bandwidth 39

G.3 Command response 40

G.4 Plant capacity 40

G.5 Measurement noise 41

G.6 Stability robustness 41

G.7 Performance robustness 41

G.8 Design goals and criteria 42

H Tustin's discretization and prewarping method 44

I Experimental and numerical results for three different afterload situations. 48

J List of symbols and subscripts 51

K Samenvatting 53

An elastance-based control scheme for a heart valve tester

L.H.M. van Gerven *, M.C.M. Rutten, M.J.G. van de Molengraft, P.H.M. Bovendeerd

Department of Biomedical Engineering, Eindhoven University of Technology, P.O. box 513, 5600 MB Eindhoven, The Netherlands

Abstract

The imitation of human heart behavior is an important issue in the field of heart physiology. Arterial pressure and flow result from the interaction between the ejecting ventricle and arterial circulation. Rutten et al. (2005) developed a bio reactor with a mock circulatory system to test aortic heart valves on their functionality by measuring pressure drops and flows. Physiological flow rate is controlled by a prescribed motion of a piston, while the aortic pressure is matched by tuning the afterload. Drawback of this setup is that valve flow does not depend on valve characteristics, but on piston motion. However, valve flow is one of the criteria in assessment of valve quality. Therefore, in this paper the heart valve tester of Rutten et al. (2005) has been extended with a control strategy for the piston motion, to better mimic the response of the heart, in terms of flow and pressure, to changes in valve properties and afterload.

The control scheme is based on the time-varying elastance model (Suga and Sagawa (1974)). The elastance control loop calculates the desired pump volume using a time-varying elastance function and the ventricular pump pressure signal. The volume control loop regulates the pump volume according to this desired pump volume.

A mathematical model of the heart valve tester has been made to show stability of the applied control algorithm, using Floquet multipliers (Parker and Chua (1989)). Furthermore, the control algorithm has been implemented on the setup. Results show that the controller is capable of responding to changes in afterload and valve properties while still generating physiological pressures and flows.

Key words: heart valve tester, control, mock circulatory system, periodic stability, elastance function.

* Corresponding author: L.H.M. van Gerven, Department of Mechanical Engineering, Eindhoven University of Technology

Email address: l.h.m.v.gerven@student.tue.nl (L.H.M. van Gerven).

1 Introduction

Mock circulatory systems (MCSs) have been widely used for evaluation of artificial hearts and ventricular assist devices (Clemente et al. (1997), Ferrari et al. (1998)). Rutten et al. (2005) developed a bio reactor with a mock circulatory system to test aortic heart valves on their functionality by measuring pressure drops and flows. Physiological flow rate is controlled with a prescribed motion of a piston, while the aortic pressure is matched by tuning the afterload. Drawback of this setup is that the valve flow does not depend on valve characteristics, but on piston motion. However, valve flow is one of the criteria in assessment of valve quality. In this paper the heart valve tester of Rutten et al. (2005) is extended with a control strategy for the piston motion to better mimic the response of the heart, in terms of flow and pressure, to changes in valve properties and afterload.

There have been several attempts reported in literature to incorporate cardiac pump function in a mock circulatory system using a time-varying elastance model (Suga and Sagawa (1974)). They describe the contraction of the ventricle in the pressure-volume plane as an elastance that varies over the cardiac cycle, the time-varying elastance model. Elastance is the ratio of intraventricular pressure and volume, i.e., a measure of cardiac muscle stiffness. In diastole, the muscle is relaxed and stiffness is low; in systole, the muscle contracts and becomes stiffer. The variable elastance model describes and analyses arterio-ventricular interaction using the End Systolic Pressure Volume Relationship (ESPVR) and Effective Arterial Elastance (EAE) curve. Changes in preload and afterload will normally result in variations of end systolic volume and pressure because the maximum value of the elastance function E_{max} remains unchanged over a wide range of afterload conditions (Maughan et al. (1984)).

Ferrari et al. (1994) made a preload-responsive mock ventricle by anticipating stroke volume, using arterial resistance, end-systolic volume, end-systolic elastance and heart rate. They used a volume control scheme guided by an adaptive reference signal. It gives physiological responses to preload changes. A disadvantage of this model is that there is no explicit control of the elastance function, i.e. no pressure-volume relationship that guides the algorithm.

Williams et al. (1994) were able to create a MCS that has the ability to mimic left ventricular pressure-volume relationships based upon a supplied time-varying elastance. It consists of two feedback loops. From pressure and volume measurements on the MCS the actual elastance is calculated and compared with a prescribed time-varying elastance (elastance feedback loop). The second loop provides control of the volume of the mock left ventricle. This MCS control scheme responds to afterload changes consistent with physiological observations. However, the pressure-volume loops of the mock ventricle show a small increase in volume at the isovolumic relaxation phase.

Baloa et al. (2001) built a mock circulatory system to mimic the Starling response of the natural heart, using Suga's elastance model. The elastance control loop calculates the desired pump pressure using the elastance function and the pump volume signal. The pressure control loop regulates the pump pressure according to this reference signal. Simulations and tests have been carried out to show the response of the elastance based controller to changes in preload, afterload and contractility. The mock ventricle shows a small

increase in volume at the isovolumic relaxation phase.
Concluding, the time-varying elastance model (Suga and Sagawa (1974)) provides good results to incorporate preload and afterload response in a MCS in spite of the problem at the isovolumic relaxation phase.
In this paper a combination of the heart valve tester of Rutten et al. (2005) and the time-varying elastance model is used to better mimic the response of the heart to changes in valve properties and afterload. Furthermore, the increase in volume at the isovolumic relaxation phase (Baloa et al. (2001), Williams et al. (1994)) is tried to be solved. It starts with a mathematical model of the heart valve tester, that shows a lumped-parameter model suited for the representation of heart-arterial interaction, a model of the cardiac valves and a model of the piston and pump. After that a control concept is treated using the pump pressure as input for the elastance model that calculates a desired pump volume (reference). The volume control loop regulates the pump volume according to this reference signal. A controlled linear servo motor drives the pump volume regulation. The controller is designed using manual loop shaping in the frequency domain. After that stability of the complete system is determined using the Floquet theory (Parker and Chua (1989)), applied to nonlinear non-autonomous time-varying periodic systems. Furthermore, the control algorithm is implemented on the experimental setup and compared with the numerically obtained control model. After that some applications are demonstrated and results are discussed.

2 Materials and concepts

2.1 Outline of the approach

The heart valve tester used in this study is the bioreactor built by Rutten et al. (2005) (figure 1). It represents the systemic circulation and consists of a computer controlled piston pump, representing the left ventricle, that generates the aortic flow rate. A terminal impedance consisting of a flexible tube and a four element windkessel (Noordergraaf et al. (1963)), that regulates the pressure. It represents the afterload. An aortic valve housing that is mounted between the pump and the flexible tube of the terminal impedance and a medium storage container representing the preload, which is connected to the pump via a mitral valve. The setup offers the possibility to measure aortic flow q_{av}, aortic pressure p_{ao}, pump pressure p_p and pump volume V_p and is mainly used to test aortic heart valves on their functionality by measuring pressure drops and flows.
Because of the differences in viscosity between blood and cell culture medium in the heart valve tester, the aortic flow and frequency of the heart cycle were reduced fourfold to impose hemodynamic similarity (Ward-Smith (1980), Rutten et al. (2005)). This reduction has been accomplished according to the scaling rules for the Navier-Stokes equations that describe the momentum and mass balance for a Newtonian incompressible fluid (Sr and Re).
In the current setup, piston motion is independent of ventricular afterload or valve prop-

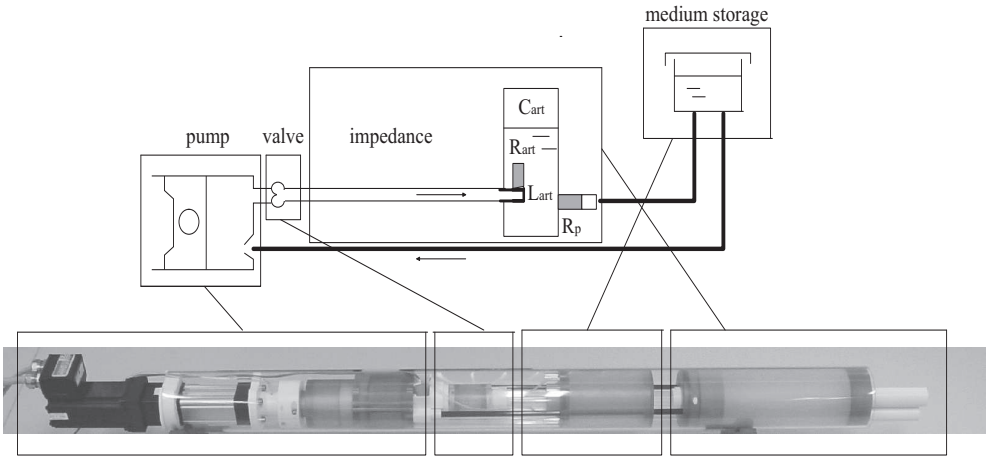

Figure 1: *The main parts of the heart valve tester. Top: schematic design, bottom: actual design.* L_{art}*,* C_{art}*,* R_{art} *and* R_p *represent the arterial inertance, arterial compliance, arterial resistance and peripheral resistance, respectively.*

erties. We want to improve the response of the heart to changes in its environment by controlling the piston motion with a time-varying elastance model that calculates a desired piston position while measuring pump pressure p_p. First a mathematical model of the setup is presented, followed by the design of the control model. The mathematical model is used to show stability of the complete system. After that the control model is implemented in the setup.

2.2 Mathematical model of the heart valve tester

The setup shown in figure 1 is modeled in three parts (figure 2). The hemodynamic preload and afterload are described with a lumped parameter model. The aortic and mitral valve are described as short tubes in which flow is dominated by inertia and the pump with piston is described as a mass with some friction.

2.2.1 Hemodynamic preload and afterload

The hemodynamic preload and afterload are described with a lumped parameter model (Sharp et al. (2000)) consisting of seven elements. This means that properties, which in real life are distributed over the whole system, are in the mathematical model lumped into a finite number of discrete components. The systemic circulation consists of three compartments: the arteries, the capillaries and the veins. The arteries and veins are modeled as constant resistances, inertances and compliances. The capillaries are modeled as a constant resistance only, which relates the pressure drop Δp to flow q. A capacitor represents the compliance of a blood vessel. It can temporarily store an amount of blood. A compliance relates changes in pressure to changes in volume. An inertance represents the inertia of the blood in the arterial and venous system. It relates the pressure drop to changes in

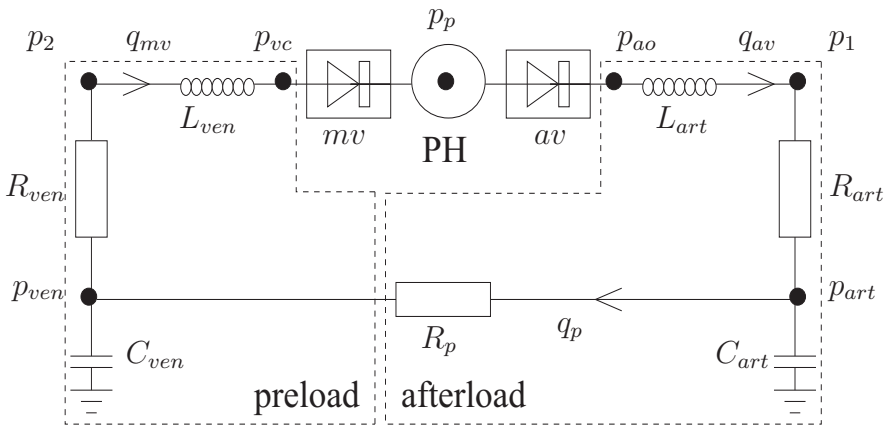

Figure 2: *Schematic representation of the heart valve tester. PH represents the pump house;* mv *and* av *the mitral and aortic valve, respectively.* R_{art}*,* R_p *and* R_{ven} *the systemic arterial, peripheral and venous resistance, respectively.* C_{art} *and* C_{ven} *the systemic arterial and venous compliance, respectively.* L_{art} *and* L_{ven} *the systemic arterial and venous inertance, respectively.* p_{ao} *and* p_{ven} *the pressure proximal to the arteries and veins, respectively.* p_{art} *and* p_{vc} *the pressure distal to the arteries and veins, respectively.* p_1 *and* p_2 *the pressure proximal to the RC parallel connection to the arteries and veins, respectively.* q_{av}*,* q_p *and* q_{mv} *are the aortic valve flow, peripheral flow and mitral valve flow, respectively,* p_p *is the pressure in the pump house.*

flow. The constitutive relations are shown in (1).

$$R = \frac{\Delta p}{q}, \qquad C = \frac{\partial V}{\partial p}, \qquad L = \frac{\Delta p}{\frac{\partial q}{\partial t}} \tag{1}$$

The differential equations representing the systemic circulation are derived from application of Kirchoff's laws, expressing conservation of mass, and momentum. They are shown in (2)-(5)

$$\frac{\partial p_2}{\partial t} = -R_{ven}\frac{\partial q_{mv}}{\partial t} + \frac{\partial p_{ven}}{\partial t} \tag{2}$$

$$\frac{\partial p_1}{\partial t} = R_{art}\frac{\partial q_{av}}{\partial t} + \frac{\partial p_{art}}{\partial t} \tag{3}$$

$$\frac{\partial p_{art}}{\partial t} = \frac{1}{C_{art}}q_{av} - \frac{1}{C_{art}R_p}p_{art} + \frac{1}{C_{art}R_p}p_{ven} \tag{4}$$

$$\frac{\partial p_{ven}}{\partial t} = -\frac{1}{C_{ven}} q_{mv} - \frac{1}{C_{ven} R_p} p_{ven} + \frac{1}{C_{ven} R_p} p_{art} \tag{5}$$

The algebraic relations for the aortic p_{ao} and vena cava p_{vc} pressure are:

$$p_{ao} = p_1 + L_{art} \frac{\partial q_{av}}{\partial t} \tag{6}$$

$$p_{vc} = p_2 + L_{ven} \frac{\partial q_{mv}}{\partial t} \tag{7}$$

2.2.2 Cardiac valves

In van den Berg et al. (2003) an equation for the flow through a valve is derived from basic fluid dynamics. The valve is modeled as a short tube with length l, in which flow is dominated by inertia. Opening and closing of the valve is simulated by changing the tube cross-sectional area A. The relation for the flow q and pressure drop Δp is shown in (8). ρ represents the medium density.

$$\frac{\partial q}{\partial t} = \frac{1}{\rho l} \Big(\Delta p A - \frac{\rho q^2}{2A} \Big) \tag{8}$$

The property of the valve to allow blood flow in one direction is modeled by assuming the valve area A to depend on the pressure difference and flow direction. The following equation is used for the valve area A:

$$A = c \cdot A_{open} + (1 - c) \cdot A_{leak} \tag{9}$$

$$c = \begin{cases} 0 \;\; q < 0 \text{ or } \Delta p < 0 \\ 1 \;\; q > 0 \text{ or } \Delta p > 0 \end{cases} \tag{10}$$

The length l of the flow channel in a valve is chosen to be equal to the square root of A_{open}. The parameter values are listed in table 1.

2.2.3 Pump and piston

The pump house of the heart valve tester can be modeled as a closed volume with two valves that generates pressures p_p, depending on the position of the piston and the flows q_{av} and q_{mv} (figure 3). Furthermore, it is assumed that the pump house has a small compliance C_p. The pressure p_p in the closed volume with two valves and a compliance can

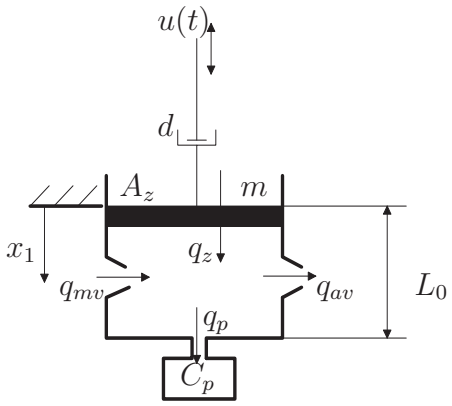

Figure 3: *Simplified model of the pump house regarded as a piston driven by the input* $u(t)$. q_{av}, q_{mv} q_p *and* q_z *represent the aortic, mitral, pump and piston flow, respectively.* x_1, A_z *and* L_0 *represent the piston position, the piston area and initial condition for the length of the piston, respectively.* C_p *represents the pump compliance.* m *and* d *represent the piston mass and damping coefficient, respectively.*

be described by analyzing the flows in the closed volume. This relation is shown in (11).

$$\frac{\partial p_p}{\partial t} = \frac{1}{C_p} q_p = \frac{1}{C_p}(A_z \dot{x_1} + q_{mv} - q_{av}) \tag{11}$$

The piston is modeled with a second-order differential equation, consisting of a mass m in combination with a friction force, modeled as a damping coefficient d and depending on the velocity x_2 of the piston.

$$\frac{\partial x_1}{\partial t} = x_2 \tag{12}$$

$$\frac{\partial x_2}{\partial t} = -\frac{d}{m} x_2 + \frac{1}{m} u \tag{13}$$

2.2.4 The time-varying elastance model

Arterial pressure and flow result from the interaction between the ventricle and the systemic circulation. Although the ventricle is neither a pressure nor a flow source, the mathematical description of its pumping function can be simple and straightforward. The contraction of the ventricle in the pressure-volume plane is described in Suga and Sagawa (1974) as an elastance that varies over the cardiac cycle.
The time-varying elastance model can be considered to describe a global cardiac muscle property. A constitutive equation for the ventricle that linearly relates ventricle volume V_{lv} to pressure p_{lv} is (figure 4, panel **A**):

$$p_{lv} = E(t)(V_{lv} - V_0) \tag{14}$$

The parameter V_0 represents the interception with the volume axis. Senzaki et al. (1996) demonstrated that after normalizing the time varying elastance curve $E(t)$ with respect to amplitude and timing of the peak, the shape is essentially constant within one species and in a large range of cardiac disease. The time-varying elastance curve $E(t)$ (15) is retrieved from this normalized curve $E_n(t_n)$

$$E(t) = E_{min} + E_n(t_n)(E_{max} - E_{min}) \tag{15}$$

when the following four parameters are known: heart rate $\frac{1}{T}$, minimal E_{min} and maximal E_{max} elastance and the time to reach maximal elastance $t_{E_{max}}$, while $t = \frac{t_n T}{t_{E_{max}}}$. The shape of $E_n(t_n)$ is shown in panel **B** of figure 4 and easily described as a finite fourier series.

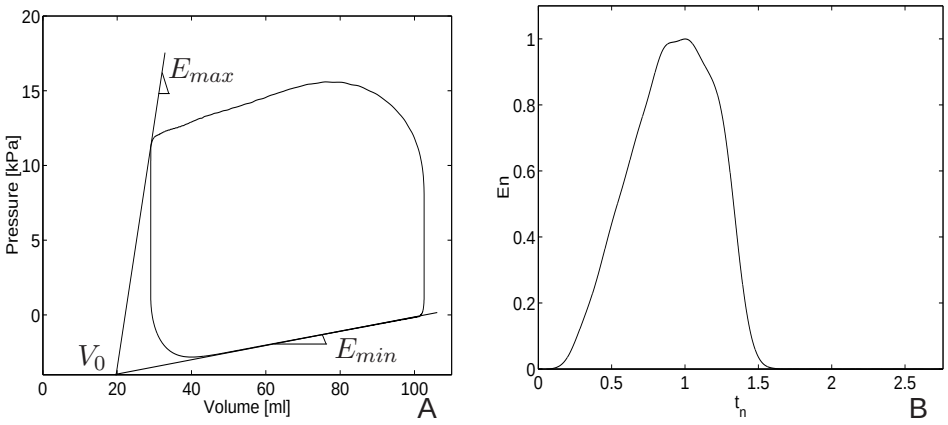

Figure 4: ***A****: Pressure-volume relationship for the left ventricle.* E_{max}*,* E_{min} *and* V_0 *represent the maximum elastance, minimum elastance and interception with the volume axis, respectively.* ***B****: Normalized elastance function.*

2.2.5 Settings of the model parameters

In this study the lumped parameter model with the $R_{art}L_{art}$ component in series is used for modeling the afterload. In the frequency domain, the afterload model can be described by its impedance which is given as:

$$Z = \frac{L_{art}R_pC_{art}s^2 + (L_{art} + R_{art}R_pC_{art})s + R_{art} + R_p}{1 + R_pC_{art}s} \tag{16}$$

At $0\,Hz$, Z equals total resistance ($R_{art} + R_p$). Its behavior at intermediate frequencies depends on the values of its system components. To assess the four parameters (C_{art}, R_{art}, L_{art} and R_p) of the afterload model (16), fourier analysis on both measured aortic

pressure p_{ao} and flow q_{av} is performed. Calculation of the ratio of flow and pressure harmonics, yields the measured input impedance. The parameter values (table 1) are found by using a simple least squares estimation technique.
The preload parameters (R_{ven}, C_{ven} and L_{ven}) (table 1) are estimated by means of trial and error because of the measurement restriction on the setup. A least squares estimation method cannot be used because the venous pressure p_{vc} cannot be measured.
The pump house of the heart valve tester has a compliance C_p. This compliance is determined by filling the pump house completely with water and sealing it. Changes in volume V_p and pressure p_p are measured while the piston is actuated with a random disturbance. From frequency response measurements $H = \frac{\partial V}{\partial p}$, the pump compliance C_p has been determined and supposed to be constant (appendix B).
The elastance function that has been designed is partly derived from recently published elastance functions (Segers et al. (2003), Suga and Sagawa (1974), Chung et al. (1997)), and partly adopted from measurements on the heart valve tester. This has been done to create physiological flow patterns in the aortic valve. The parameter values are listed in table 1.

Table 1: *Parameter values for the mathematical model.*

$L_{art}\ (Pa \cdot s^2 \cdot m^{-3})$	$1.81 \cdot 10^5$	$\rho\ (kg \cdot m^{-3})$	$1.05 \cdot 10^3$	$L_0\ (m)$	0.045
$C_{art}\ (m^3 \cdot Pa^{-1})$	$1.26 \cdot 10^{-8}$	$l_{mv}\ (m)$	$2.7 \cdot 10^{-2}$	$m\ (kg)$	0.045
$R_{art}\ (Pa \cdot s \cdot m^{-3})$	$1.84 \cdot 10^7$	$l_{av}\ (m)$	$2.1 \cdot 10^{-2}$	d	0.5
$R_p\ (Pa \cdot s \cdot m^{-3})$	$4 \cdot 10^8$	$A_{open,av}\ (m^2)$	$4.5 \cdot 10^{-4}$	$E_{max}\ (kPa \cdot ml^{-1})$	2.54
$L_{ven}\ (Pa \cdot s^2 \cdot m^{-3})$	$7 \cdot 10^1$	$A_{open,mv}\ (m^2)$	$7.2 \cdot 10^{-4}$	$E_{min}\ (kPa \cdot ml^{-1})$	$4.79 \cdot 10^{-2}$
$C_{ven}\ (m^3 \cdot Pa^{-1})$	$3 \cdot 10^{-5}$	$A_{leak,av}\ (m^2)$	$4.5 \cdot 10^{-8}$	$T\ (s)$	3.2
$R_{ven}\ (Pa \cdot s \cdot m^{-3})$	$6 \cdot 10^7$	$A_{leak,mv}\ (m^2)$	$7.2 \cdot 10^{-8}$	$t_{E_{max}}\ (s)$	1.16
$C_p\ (m^3 \cdot Pa^{-1})$	$2.45 \cdot 10^{-10}$	$A_z\ (m^2)$	$2.21 \cdot 10^{-3}$	$V_0\ (m^3)$	$19.6 \cdot 10^{-6}$

2.3 Control concept

The control concept (figure 5) is based on feedback of the pump volume V_p [1], which is related to the position of the piston x_1. The elastance control loop calculates the desired piston position x_{des} using the time-varying elastance function and the pump pressure p_p. The volume control loop regulates the piston position x_1 according to this desired reference position x_{des}.

[1] Another possible control concept, which uses pump pressure p_p for feedback, is treated in appendix C.

The desired reference signal x_{des} (17) is derived from the pump pressure p_p through the time-varying elastance model (14) and the geometrically properties of the pump (figure 3).

$$x_{des} = L_0 - \frac{1}{E(t)A_z}p_p - \frac{V_0}{A_z} \tag{17}$$

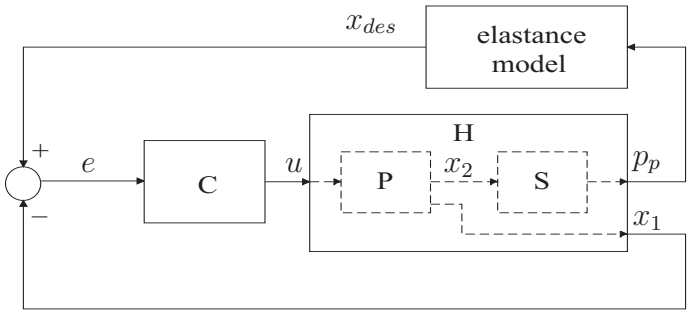

Figure 5: *Block diagram where position of the piston x_1 is used for feedback. x_2 and e represent the piston velocity and error $x_{des} - x_1$, respectively. x_{des}, p_p and u represent the desired piston position, the pump pressure and the input for the system, respectively. C represents the controller, H the total open loop system, i.e. the heart valve tester with the piston and pump P, valves and hemodynamic preload and afterload S.*

2.3.1 Servo controller

In the linear control theory the most common method for an indication of the system behavior is the frequency response design method (FRF). For the design of the servo controller marked with 'C' (figure 5), manual loop shaping of the open loop FRF in the frequency domain is used (Franklin et al. (1996), Bosgra et al. (2003)). The designed controller consists of a lead compensator with an integral action. The lead compensator takes care of the required phase advance in the resonance frequency region, preserving stability and robustness. The integral action takes care of the disturbance rejection, i.e. suppression of the low frequency disturbances. For measurement noise reduction and high frequency robustness a second order high frequency roll-off compensator has been used. The open loop transfer function has a bandwidth of $30\,Hz$ with a phase advance of 45° at $0\,dB$ cross-over frequency (figure 6, panel **A**). The Nyquist plot of the open loop gain shows stability and robustness (figure 6, panel **B**). This controller design generates typical piston trajectories with error margins smaller than 0.3 *mm* (figure 6, panel **C** and **D**). A detailed explanation of the servo controller design is described in appendix E.

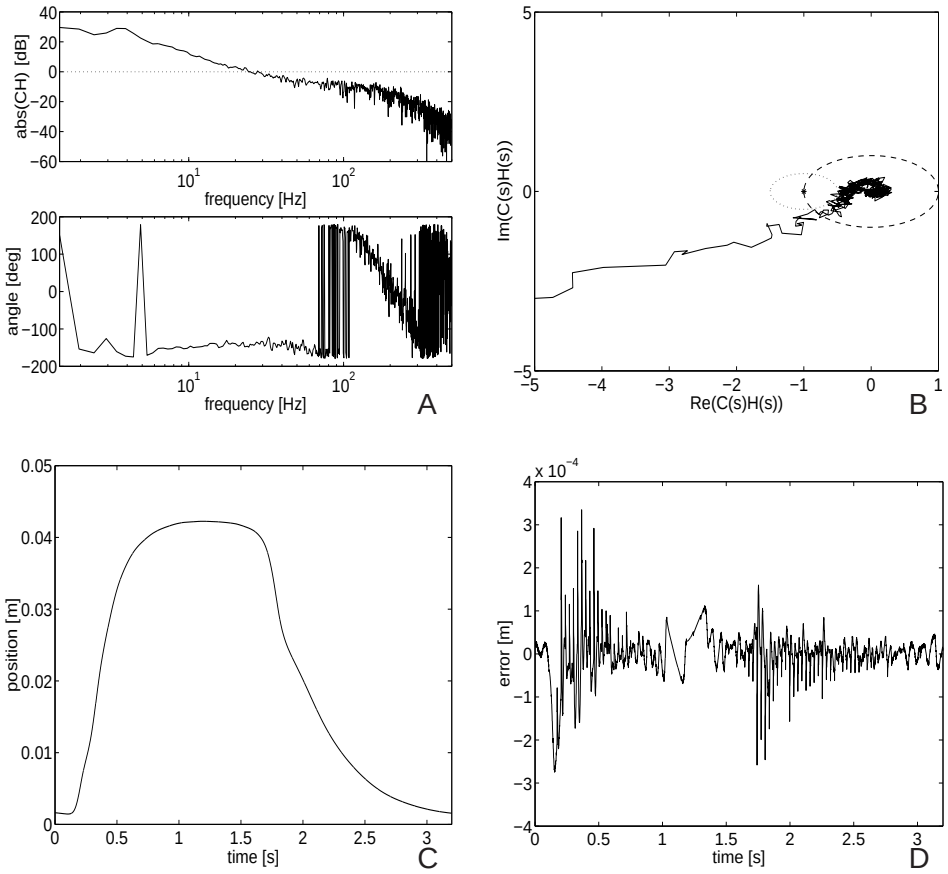

Figure 6: ***A****: Open loop frequency response.* ***B****: Nyquist plot of the open loop response.* ***C****: Reference piston position x_{des} trajectory.* ***D****: Error signal between reference and tracked position signal.*

2.3.2 Stability

For analyzing the stability of the complete control model a strategy applied to nonlinear non-autonomous time-varying systems with a periodic solution is used. The Floquet theory gives information on the stability of the periodic solution of this system (Parker and Chua (1989)). The stability of the complete system is determined by its characteristic multipliers, also called Floquet multipliers, i.e. eigenvalues of the monodromy matrix Φ_T. In this matrix the fundamental solutions of the periodic system are stored. The Floquet multipliers determine the exponential growth or decay of perturbations in the eigendirections of the monodromy matrix Φ_T and hence the stability of the periodic solution. If a Floquet multiplier has a magnitude larger (smaller) than one, a perturbation of the initial condition in the corresponding eigendirection will grow (decay) after one period of oscillation.
The monodromy matrix for the complete control model has been determined by the Newton-Raphson shooting method (Leine and van de Wouw (2002)). The Floquet multipliers, belonging to this monodromy matrix, show that the system is marginally stable. Three Floquet multipliers have a value 1. This means that if a disturbance is applied to the system in the direction of the eigenvector belonging to one of these Floquet multipli-

ers, the applied disturbance is not vanishing nor increasing but remains on the periodic solution. A detailed explanation of this method is described in appendix D.

2.4 Implementation of the control concept

2.4.1 Data acquisition

The concept described above is implemented in the heart valve tester setup. The data acquisition is performed by a *TUeDACS/1* (TU/e, The Netherlands) system which is connected to a *BLH30* Brushless servo drive in combination with a *ML2340* DC servo motor (Parker, The Netherlands). The piston position is measured with quadrature encoders. These encoders have an accuracy of 2000 *pulses/cycle*. For measuring the aortic and pump pressure *Becton Dickinson P10EZ-1* pressure sensors are used. The aortic flow is measured by a *MC 28AX* flow probe connected to a flow meter *TS420* (both Transonic, The Netherlands).

2.4.2 Initialization

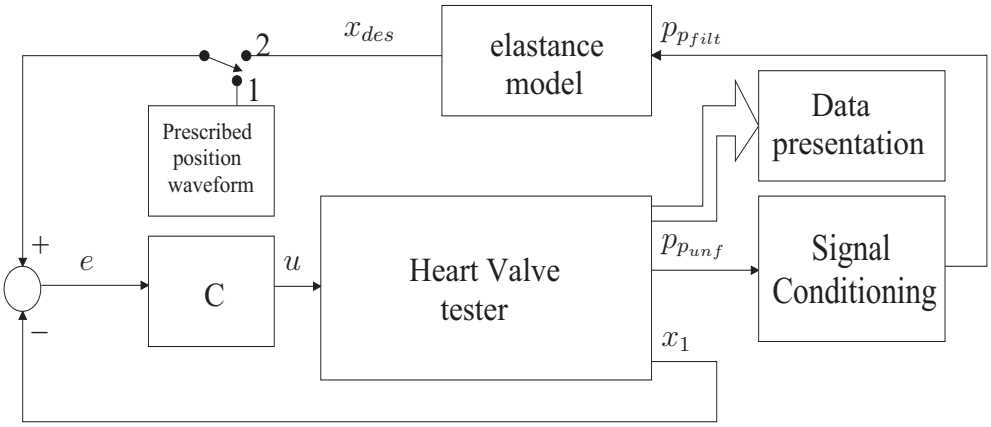

Figure 7: *Schematic block diagram for implementation of the control algorithm in the heart valve tester.* x_1 *and* e *represent the piston position and error* $x_{des} - x_1$*, respectively.* x_{des}*,* $p_{p_{unf}}$ *and* u *represent the desired piston position, the unfiltered pump pressure and the input for the system, respectively.* $p_{p_{filt}}$ *represents the filtered pump pressure.*

To facilitate the initialization of the algorithm, it is necessary to divide the startup process into two stages (figure 7). In stage 1 the heart valve tester operates under the control of the volume loop only. The reference position is prescribed using a prescribed position waveform to have physiological pressures and flows before the elastance control loop is activated (stage 2). This occurs at the moment the prescribed position waveform and desired position x_{des} are matching. The elastance control loop thereafter dynamically calculates the piston position using the time-varying elastance function and instantaneous pump pressure $p_{p_{filt}}$.

2.4.3 Signal conditioning

To produce a smooth desired piston position x_{des}, signal conditioning is applied to the measured pump pressure $p_{p_{unf}}$ because it contains too much undesired noise (figure 8, panel **A**). Investigation of the power spectrum of this signal (panel **B**) shows for frequencies larger than $5\,Hz$ uncorrelated noise. Furthermore, a small increase in the PSD spectrum can be seen at $30\,Hz$, the system's bandwidth. Therefore, second order filtering has been applied to smooth the pump pressure. This filter has a time dependent cut-off frequency that fluctuates between $5\,Hz$ during ejection phase and $1.5\,Hz$ during filling phase of the pump. The cut-off frequency of this filter is decreased from $5\,Hz$ to $1.5\,Hz$ because of the relative low pump pressure during filling phase which means that uncorrelated noise becomes more relevant. The filtered pump pressure $p_{p_{filt}}$ and PSD spectrum, belonging to this filtered pump pressure, are shown in panel **C** and **D** of figure 8.
Furthermore, the measured flows and pressures plotted in this paper are zero phase filtered (ZPF) to be able to analyze the obtained results better.
The control algorithm has been tested numerically as well as experimentally for one afterload setting to validate experimental data with simulation data. For this experiment a

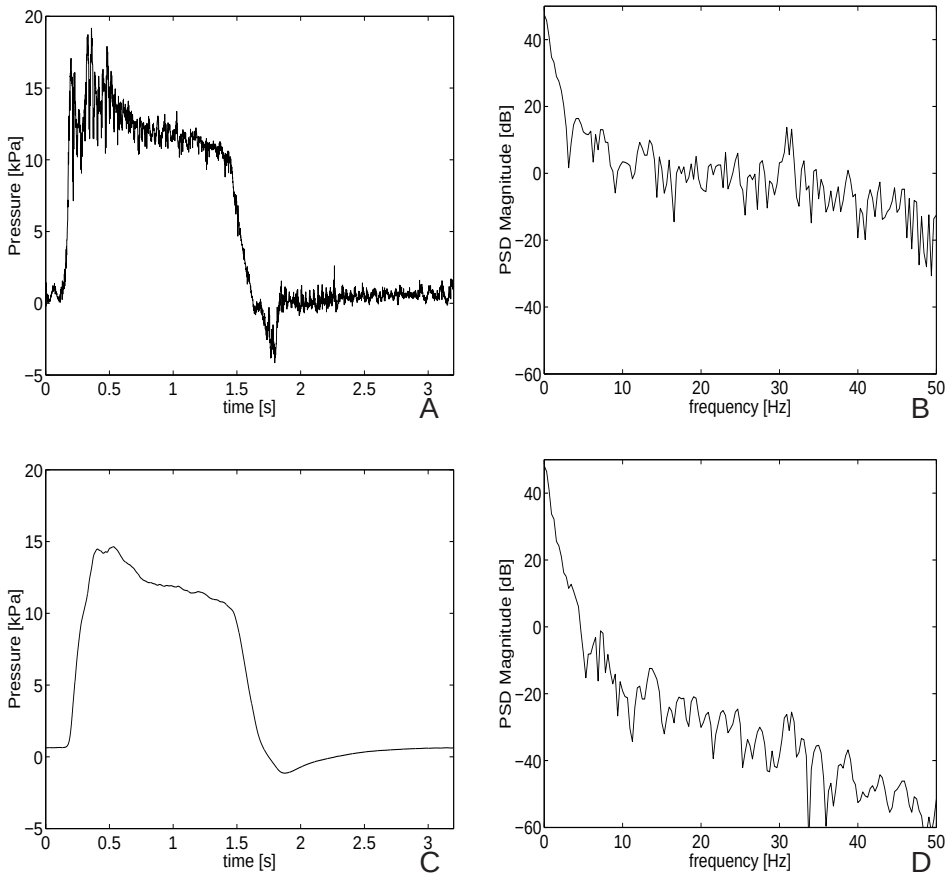

Figure 8: ***A**: Unfiltered pump pressure $p_{p_{unf}}$ for one cardiac cycle. **B**: Power spectrum density (PSD) belonging to the unfiltered pump pressure. **C**: Filtered pump pressure $p_{p_{filt}}$ for one cardiac cycle. **D**: Power spectrum density belonging to the filtered pump pressure.*

bioprosthetic aortic valve (*Medtronic Freestyle 995*) with a nominal diameter of 21 *mm* was used. To test the functionality of the controlled circulation model pressure-volume relations ($P - V$ loops) were measured for four different peripheral resistance levels of the afterload. Subsequently, the aortic valve was replaced by another (bioprosthetic) aortic valve to check the effect of different heart valves on the pump behavior. Both valves were taken from the same batch of stentless bioprosthetic heart valves, one having a low flow resistance, the other one having a higher resistance.

3 Results

The comparison of numerical and experimental data for one afterload setting is depicted in figure 9. The afterload impedance Z of experimental data, simulated data and estimated impedance (16) is shown in panel **A** of figure 9. At 0 *Hz* its values are consistent with the total resistance ($R_{art} + R_p$).
For both the experimental and simulated data the maximal pump pressure is approximately 16 *kPa*, while the maximal aortic pressure is somewhat lower (figure 9, panel **B**). A significant difference between simulation and experiment is shown in the early filling phase marked with 1. A second difference is the fact that the experimental aortic $p_{ao_{exp}}$ and pump $p_{p_{exp}}$ pressures show oscillations during the ejection phase, marked with 2. The experimental and simulated aortic q_{av} and mitral q_{mv} flows are shown in panel **C** of this figure. The mitral flow cannot be measured directly from the setup but is calculated by means of the relation in (11). In both cases (simulation and experiment) the maximal flow across the aortic valve is higher than the maximal flow across the mitral valve. However, there is a difference in maximum mitral flow during diastole, marked with 3. Furthermore, the experimental mitral flow $q_{av_{exp}}$ becomes negative at the beginning of the contraction phase, marked with 4. The cardiac volume is minimal at end systole and maximal at end diastole (figure 9, panel **D**). A difference between experimental and simulated data can be seen in end diastole cardiac volume, marked with 5.
The experimental (panel **A**) and simulated (panel **B**) $P - V$ loops generated with varying afterloads are depicted in figure 10. The estimated afterload parameters belonging to these responses are shown in table 2. Both in simulation and experiment maximum pump pressure and minimum pump volume rise with increasing afterload. The isovolumic contraction phase and the isovolumic relaxation phase can be distinguished at the maximal and minimal values of the cavity volumes. The values of E_{max} in both experimental and simulated results are estimated by the slope of the points with the highest pressure-volume ratio and were found to be $1.34\ kPa \cdot ml^{-1}$ and $1.58\ kPa \cdot ml^{-1}$, respectively. In both figures E_{max} is maintained constant. This demonstrates the fact that the control algorithm is able to maintain a constant contractility state in the presence of changing afterloads. The remaining results for the different afterload levels are presented in figures I.1-I.3 in appendix I.
Finally responses to changes in aortic valves have been demonstrated to show the effect of the control algorithm (figure 10, panel **C**). The valve with higher resistance clearly in-

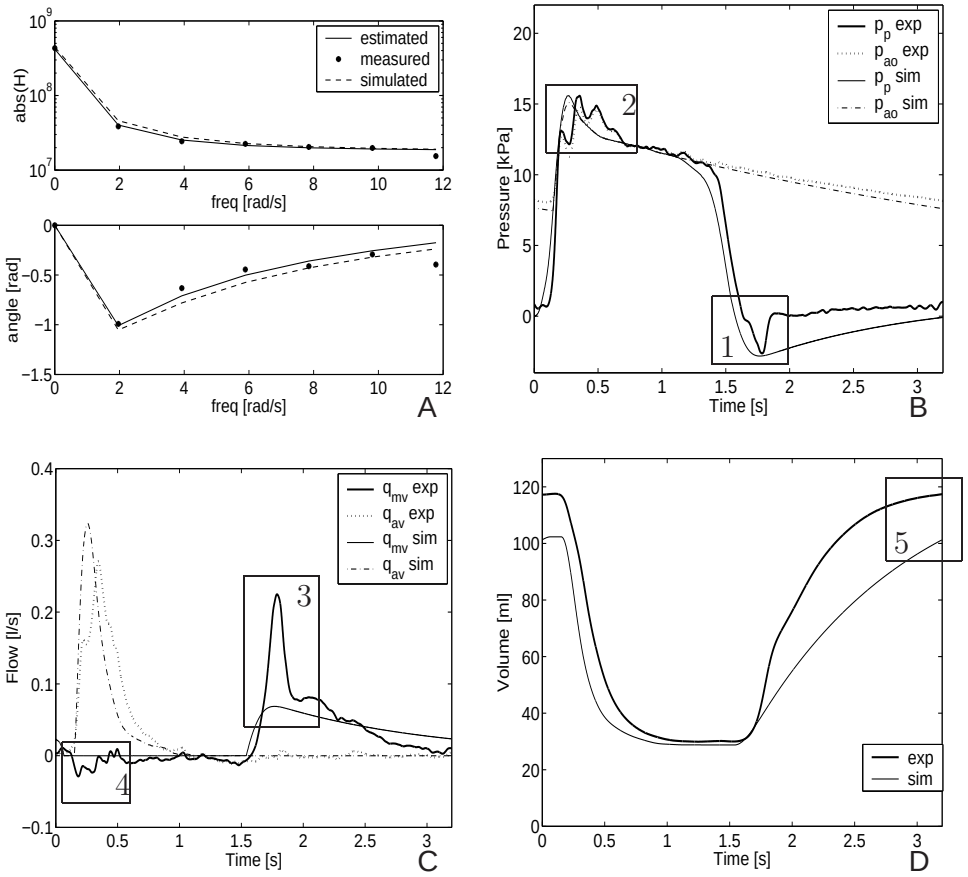

Figure 9: ***A****: Frequency response function of the afterload impedance* Z. ***B****: Numerically(sim) and experimentally(exp) obtained pump pressure* p_p *and aortic pressure* p_{ao} *for one cardiac cycle.* ***C****: Aortic* q_{ao} *and mitral* q_{mv} *flow.* ***D****: Volume as a function of time calculated by the integration of volume change in aortic and mitral flow.*

creases the work load of the heart valve tester.

Table 2: *Parameter values for the systemic circulation for four different afterload levels.*

	L_{art}	C_{art}	R_{art}	R_p
exp 1	$3.17 \cdot 10^5$	$1.36 \cdot 10^{-8}$	$2.15 \cdot 10^7$	$2.63 \cdot 10^8$
exp 2	$1.81 \cdot 10^5$	$1.26 \cdot 10^{-8}$	$1.84 \cdot 10^7$	$1.00 \cdot 10^8$
exp 3	$3.13 \cdot 10^5$	$1.34 \cdot 10^{-8}$	$1.77 \cdot 10^7$	$5.30 \cdot 10^8$
exp 4	$1.25 \cdot 10^5$	$1.22 \cdot 10^{-8}$	$1.90 \cdot 10^7$	$7.43 \cdot 10^8$

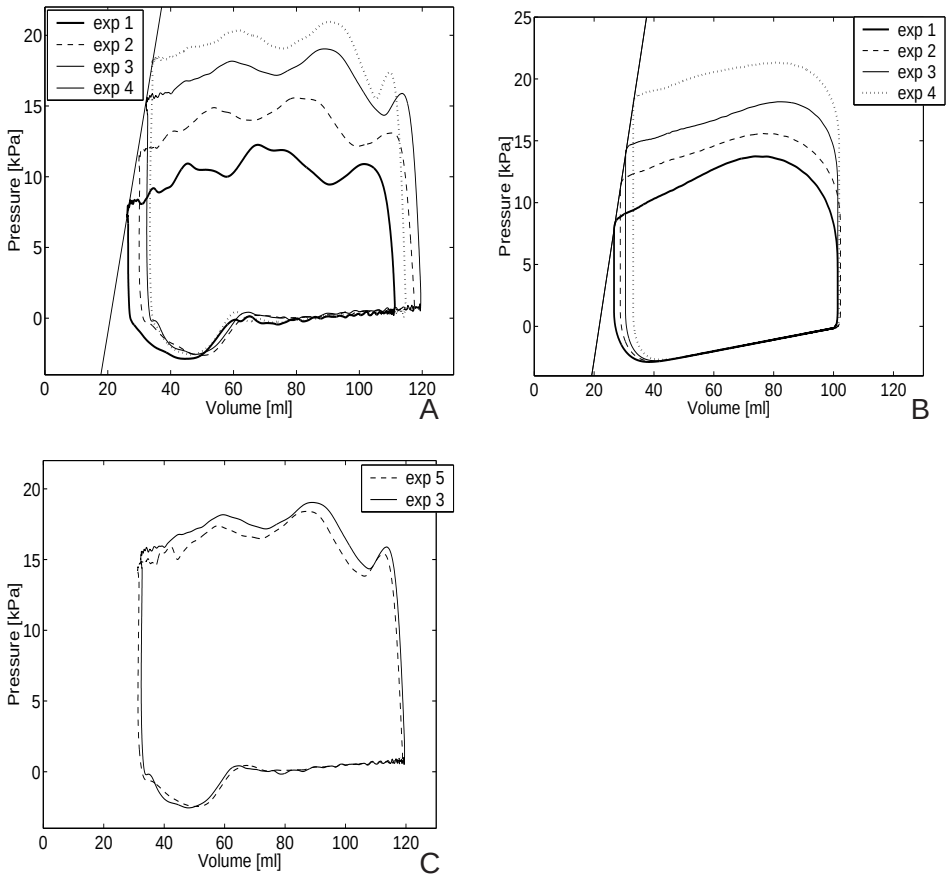

Figure 10: *Experimentally (**A**) and numerically (**B**) obtained pressure-volume curves for the four different afterload settings. **C**:Experimentally obtained pressure-volume curves for two different aortic valves.*

4 Discussion

In this article a control strategy for the heart valve tester has been developed, that mimics the physiological response of the heart in terms of pressures and flows to changes in hemodynamic load.

A ninth order system of ordinary differential equations has been used as a mathematical model for the mock circulatory system to evaluate the control algorithm. A limitation of this description is that it simplifies the fluid dynamic behavior by using a lumped parameter model to describe what is actually a continuous system. However, the model is found to describe the hemodynamics of the system adequately under the conditions studied.

The designed servo controller preserves stability and robustness. Furthermore, marginal stability for the complete system has been guaranteed using a stabilization method applied to nonlinear time-varying systems with a periodic solution.

The incorporation of an initialization sequence has been effective to have physiological pressures and flows at the moment the elastance control loop is activated.

Signal conditioning of the pump pressure $p_{p_{unf}}$ has been carried out to produce a smooth

desired piston position x_{des}. The power spectrum shows uncorrelated noise for frequencies larger than $5\,Hz$. This noise can be attributed to measurement noise in the pressure sensor and uncorrelated high frequent noise in the servo drive system. The small increase in PSD spectrum at $30\,Hz$ cannot be declared. If this small increase was related to a system property, it would be visible in the open loop transfer function at frequency $30\,Hz$ (panel **A** of figure 6). Due to a stiff construction of the heart valve tester, small external deviations in the servo drive lead to large variations in pressure. Together with measurement noise in the pressure sensor, signal conditioning was needed to obtain a smooth desired piston position x_{des}.

The numerical and experimental results (figure 9) match relatively well, although there are some differences visible. The estimation of the afterload impedance Z (16) has been performed and is matching well for both simulation and experiment (panel **A**). First of all, there is a difference in pressure dip at the end of the contraction phase (panel **B** (1)). This may be attributed to the low (and unadjustable) preload of the heart valve tester. Secondly, the pressure oscillations of the measured data during the ejection phase (panel **B** (2)). This can be related to the stiff construction of the heart valve tester setup and the measurement noise in the pressure sensors. The difference in mitral flow in the diastolic phase (panel **C** (3)) can be contributed to the chosen preload parameters in the numerical control model. They cannot be estimated due to restrictions in the construction of the heart valve tester. For this reason they are estimated by trial and error. These preload parameters have large influence on the mitral flow q_{mv}, and thus the diastolic phase, i.e. filling of the ventricle and determination of the end-diastolic volume (panel **D** (5)). Furthermore, the negative mitral flow $q_{mv_{exp}}$ (panel **C** (4)) means a small leakage of the mitral valve at the moment the contraction phase starts.

Panel **A** and **B** of figure 10 show that the E_{max} in simulation and experiment are linearly dependent on end-systolic volume, i.e. insensitive to afterload changes. These results show that a reduction of cardiac output occurs when contractility of the ventricle remains constant and afterload is increased. This is similar to *in vivo* obtained results (Maughan et al. (1984)). The values of E_{max} in both experimental and simulated results were found to be $1.34\ kPa \cdot ml^{-1}$ and $1.58\ kPa \cdot ml^{-1}$, respectively. These values differ significantly with the $E_{max} = 2.54\ kPa \cdot ml^{-1}$ of the elastance function. An explanation for this fact is not known.

From the obtained results in panel **C** of figure 10, the control algorithm provides not only realistic responses with respect to changes in hemodynamic afterload but can also provide good information for testing the functionality of aortic heart valves. It shows a difference in cardiac volume and pressure to a change in aortic valve. Despite the imperfections shown above, the effect of changes in valve properties and afterload on pump pressure and volume is clearly demonstrated.

Baloa et al. (2001) and Williams et al. (1994) managed to design control schemes that were able to respond to afterload changes as well. However, these $P - V$ loops showed an increase in volume at the isovolumic relaxation phase. In this paper this problem has been solved (figure 10) using the piston position x_1 for feedback instead of the pressure p_p or elastance $E(t)$.

5 Conclusion

The heart valve tester of Rutten et al. (2005) has been extended with a control strategy to better mimic the response of the heart in terms of pressures and flows to changes in afterload and valve properties. It has been accomplished using the time-varying elastance model to calculate a desired pump volume from measurements on the pump pressure. The volume control loop regulates the pump volume according to this reference signal.
Future development of the mathematical and mock circulatory system would benefit from the addition of more complex heart behavior, such as a baraoreflex response to regulate heart rate (Lu et al. (2001)).

References

L. A. Baloa, J. R. Boston, and J. F. Antaki. Elastance-based control of a mock circulatory system. *Annals of biomedical engineering*, 29:244–251, 2001.

J. Boot, M. J. G. van de Molengraft, and P. W. J. M. Nuij. Frequency response measurement in closed loop: brushing up our knowledge(w 2003.59). Eindhoven University of Technology Department of Mechanical Engineering, 2003.

O. H. Bosgra, H. Kwakernaak, and G. Meinsma. Design methods for control systems. Dutch Institute of Systems and Control(DISC), Winter 2003.

D. Chung, S. Niranjan, J. W. Clark, A. Bidani, W. E. Johnston, J. B. Zwischenberger, and D. L. Traber. A dynamic model of ventricular interaction and pericardial influence. *American Journal of Physiology, Heart Circulation Physiology*, 272:H2942–H2962, 1997.

F. Clemente, G. Ferrari, C. D. Lazzari, and G. Tosti. Technical standards for medical devices: Assisted circulation devices. *Technology and Health Care*, 5:19–34, 1997.

G. Ferrari, C. D. Lazzari, R. Mimmo, D. Ambrosi, and G. Tosti. Mock circulatory system for in vitro reproduction of the left ventricle, the arterial tree and their interaction with a left ventricular assist device. *J. Med. Eng. Technol*, 18:87–95, 1994.

G. Ferrari, C. D. Lazzari, R. Mimmo, G. Tosti, D. Ambrosi, and K. Gorczynska. A computer controlled mock circulatory system for mono and biventricular assist device testing. *Int. J. Artif. Organs*, 21:26–36, 1998.

G. F. Franklin, J. D. Powell, and A. Emamai-Naeini. *Feedback control of dynamic systems*. Addison-Wesley, New York, 1996. ISBN 0-201-53487-8.

A. C. Guyton and J. E. Hall. *Textbook of Medical Physiology*. W.B. Saunders Company, 9th edition, 1996.

R. I. Leine and N. van de Wouw. Numerical methods for computing periodic solutions: Lecture notes of the course nonlinear dynamics 4j520. Eindhoven University of Technology Department of Mechanical Engineering, 2002.

K. Lu, J. W. Clark, F. H. Ghorbel, D. L. Ware, and A. Bidani. A human cardiopulmonary system model applied to the analysis of the valsalva maneuver. *American Journal of Physiology, Heart Circulation Physiology*, 281:H2661–H2679, 2001.

W. L. Maughan, K. Sunagawa, D. Burkhoff, and K. Sagawa. Effect of arterial impedance changes on the end-systolic pressure-volume relation. *Cirulation Research*, 54:595–602, 1984.

A. Noordergraaf, G. N. Jager, and N. Westerhof. *Circulatory analog computers*. North Holland Publishing Co., Amsterdam, 1963.

T. S. Parker and L. O. Chua. *Practical numerical algorithms for chaotic systems*. Springer-Verlag, New York, 1989.

M. C. M. Rutten, M. W. Wijlaars, A. Mol, E. A. van Dam, G. J. Strijkers, K. Nicolay, and F. P. T. Baaijens. The valve exerciser: A novel bioreactor for physiological loading of tissue-engineered aortic valves. submitted to Journal of Biomechanics, 2005.

S. Sastry. *Nonlinear systems: analysis, stability and control*. Springer-Verlag, New York, 1999. Interdisciplinary Applied Mathematics.

P. Segers, N. Stergiopulos, N. Westerhof, P. Wouters, P. Kolh, and P. Verdonck. Systemic and pulmonary hemodynamics assessed with a lumped-parameter heart-arterial interaction model. *Journal of Engineering Mathematics*, 43:185–199, 2003.

H. Senzaki, C. H. Chen, and D. A. Kass. Single-beat estimation of end-systolic pressure-volume relation in humans. a new method with the potential for noninvasive application. *Circulation 94*, pages 2497–2506, 1996.

B. Shahian and M. Hassul. *Control system design using Matlab*. Prentice-Hall, 1993. ISBN 0-13-174061-X.

M. K. Sharp, G. M. Pantalos, L. Minich, L. Y. Tani, E. C. McGough, and J. A. Hawkins. Aortic input impedance in infants and children. *J Appl Physiol*, (88):2227–2239, 2000.

H. Suga and K. Sagawa. Instantaneous pressure-volume relationships and their ratio in the excised, supported canine left ventricle. *Circulation research*, 35:117–126, 1974.

P. M. J. van den Berg, P. H. M. Bovendeerd, F. N. van de Vosse, M. C. M. Rutten, N. H. J. Pijls, T. Arts, M. C. F. Geven, and N. Westerhof. Intramyocardial pressure and its influence on the coronary circulation (bmte 03.34). Master's thesis, Eindhoven University of Technology Department of Biomedical Engineering, 2003.

A. Ward-Smith. *Internal Fluid Flow*. Clarendon Press, Oxford, 1980.

J. L. Williams, J. F. Antaki, J. R. Boston, S. L. Williams, J. C. Woodard, P. J. Miller, and R. L. Kornos. Load sensitive mock circulatory system for left ventricular assist device controller evaluation and development. *Proceedings of the 16th Annual International Conference of the IEEE Engineering in Medicine and Biology Society*, pages 89–90, 1994.

A Anatomy and physiology of the heart

The heart is a hollow muscular organ that pumps blood through the vascular system for transport of oxygen and nutrients. It consists of two pumps, the right and left heart which are shown in figure A.1. Both sides contain an atrium and a ventricle. The atria collect blood that returns to the heart and facilitate rapid filling of the ventricles. The ventricle supplies the main force that pumps the blood through either the pulmonary or the systemic circulation. The wall of the right ventricle is less powerful than that of the left ventricle. The mitral valve prevents back flow of blood into the left atrium when the left ventricle contracts and blood is ejected through the aortic valve. The aortic valve prevents back flow of blood from the aorta into the left ventricle. The tricuspid valve prevents back flow of blood into the right atrium when the right ventricle contracts and blood is ejected through the pulmonary valve. The pulmonary valve prevents back flow from the pulmonary artery to the right ventricle. The cardiac event that occurs from the beginning of one heartbeat to

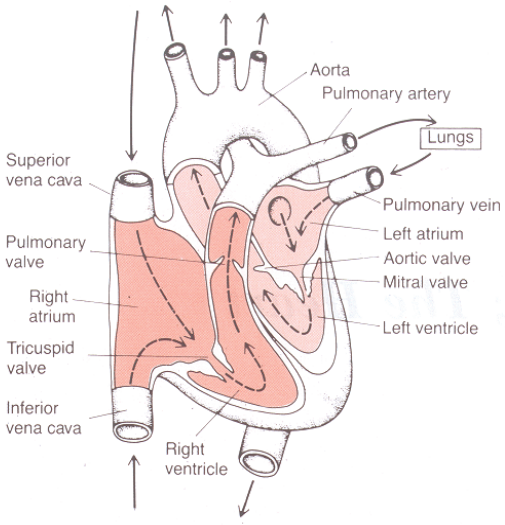

Figure A.1: *The structure of the heart and course of blood flow through the heart chambers, adopted from Guyton and Hall (1996)*

the beginning of the next is called the cardiac cycle. Each cycle is initiated by spontaneous generation of an action potential from the sinus node, which is located in the superior lateral wall of the right atrium near the opening of the superior vena cava. This action potential travels rapidly through both atria and thence into the ventricles. The cardiac cycle can be divided into four individual phases. In the first phase, the filling phase, relaxation of the heart muscle enables the ventricle to be filled with blood from the atria. During the next isovolumic contraction phase the ventricles start to contract without volume changes. The pressure into the ventricles starts to rise until the ventricles have built up sufficient pressure to push the valve open against the pressure in the aorta or pulmonary artery. This moment marks the beginning of the ejection phase during which blood pours out of the ventricles. As soon as the flow tends to become negative, the aortic of pulmonary valve closes and the isovolumic relaxation phase begins. The period of relaxation is called diastole, during

which the heart fills with blood. The period of contraction is called systole.

B Determination of pump compliance C_p

The pump house of the heart valve tester setup has a certain compliance C_p. This compliance relates changes in pressure to changes in volume. This parameter has to be known for use in the mathematical model of the heart valve tester (11). Furthermore, because this parameter is supposed to be known for calculation of the mitral flow q_{mv}, by measuring the aortic flow q_{av} and pump pressure p_p.
This compliance is determined by filling the pump house completely with water and sealing it. Changes in volume V_p and pressure p_p are measured while the piston is actuated with a random disturbance. The frequency response function of $H = \frac{\partial p}{\partial V}$ can now be determined.
The experiment is carried out by measuring frequency response functions at three different piston positions in the pump housing; at almost maximum volume V_p, at half the maximum volume and almost minimum volume. In figure B.1 the frequency responses and their coherence functions are shown. In all three cases it is shown that in the low frequency area (working area of the valve tester), the inverse of the compliance $\frac{\partial p}{\partial V}$ is almost constant. Concluding, the pump compliance C_p is supposed to have a constant value of $2.45 \cdot 10^{-10}\ m^3 \cdot Pa^{-1}$.

C Concept with feedback of pump pressure p_p

This concept is based on feedback of pump pressure p_p, which is related to the position of the piston x_1.. The piston position x_1, is put into the time-varying elastance model and calculates a desired pressure p_{lv}. The pressure control loop regulates the pump pressure p_p according to this desired reference pressure p_{lv}. The basic block diagram for this control strategy is shown in figure C.1. From the nonlinear feedback theory there is a known method called input-output linearization for SISO systems using Lie-derivatives (Sastry (1999)). Given the single-input single-output system

$$\dot{x}(t) = f(x) + g(x)u$$

$$y = h(x) \tag{C.1}$$

with f, g smooth vector fields and h a smooth nonlinear output function, then the Lie-derivative $L_f h(x)$ or $L_g h(x)$ gives the rate of change of h along the flow of the vector field f or g. This method transforms a nonlinear system into a simple linear normal form by means of a change of coordinates. Writing the system into this normal form is much

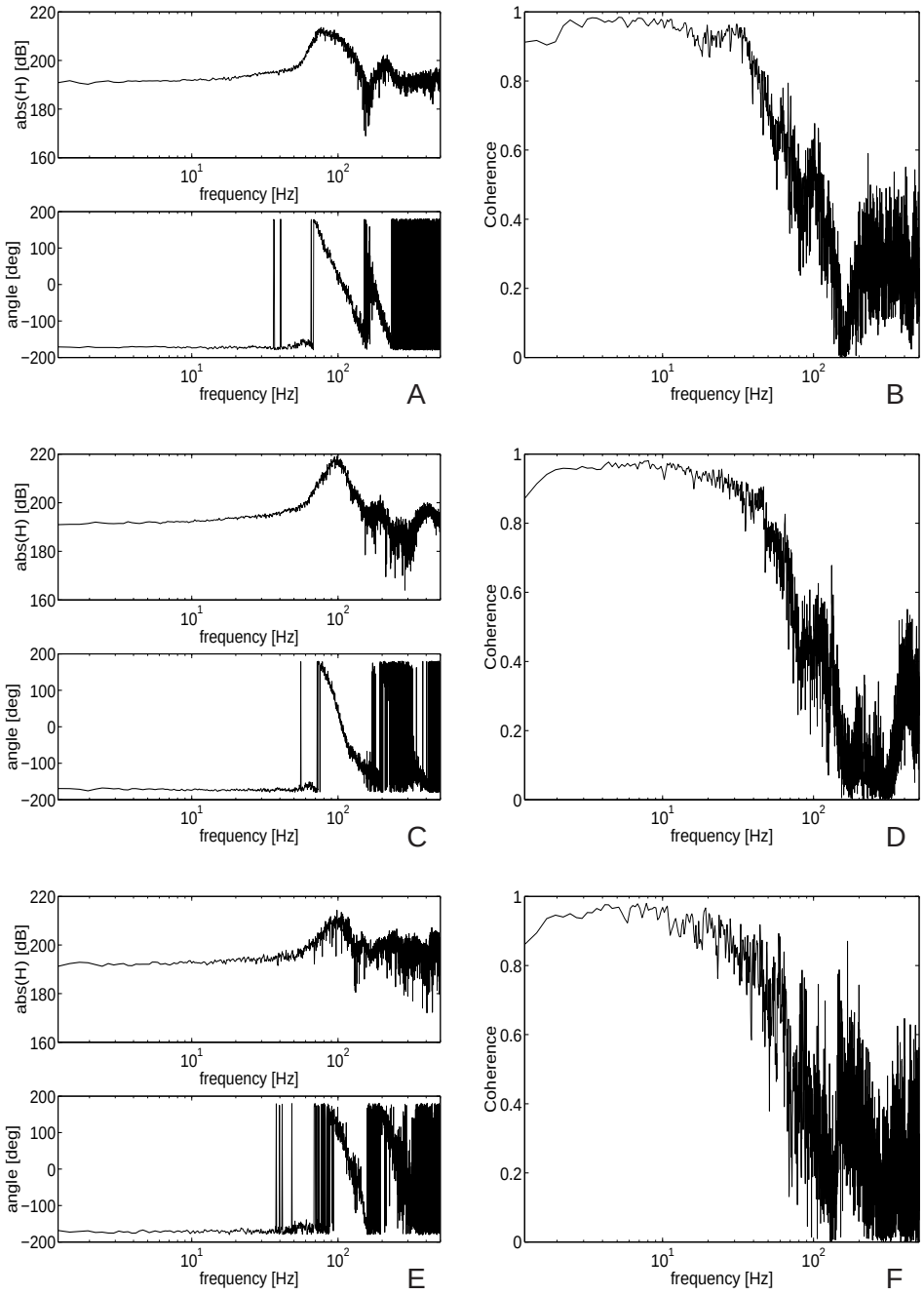

Figure B.1: ***A**: Bode diagram of pressure p_p and volume V_p for determine the compliance C_p for the piston positioned at almost maximum closed volume. **B**: Coherence function belonging to bode diagram in panel **A**. **C**: Bode diagram of pressure p_p and volume V_p for the piston positioned at half of maximum closed volume. **D**: Coherence function belonging to bode diagram in panel **C**. **E**: Bode diagram of pressure p_p and volume V_p for the piston positioned at almost minimum closed volume. **F**: Coherence function belonging to bode diagram in panel **E**.*

easier in designing controllers and understand the dynamics in nonlinear systems. It is now possible to use standard linear feedback theory for designing an input u.

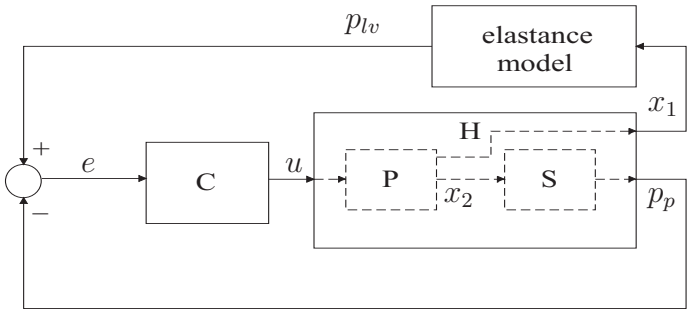

Figure C.1: *Block diagram where pump pressure p_p is used for feedback. x_1, x_2 and e represent the piston position, piston velocity and error, respectively. p_{lv}, p_p and u represent the desired pump pressure, the pump pressure and the input for the system, respectively. C,H,P and S represent the controller, the total open loop system, the piston with pump and the systemic circulation, respectively.*

The output function is assumed to be given by $y = h(p) = p_p$. Then, the strict relative degree of the system is 2, consisting of:

$$
\begin{aligned}
y &= h(p) = p_p \\
\dot{y} &= L_f h(p) + L_g h(p) = \tfrac{1}{C_p}\Big(A_z x_2 + q_{mv} - q_{av}\Big) \\
\ddot{y} &= L_f^2 h(p) + L_g^2 h(p) = \tfrac{1}{C_p}\Big(A_z\Big(-\tfrac{d}{m}x_2 + \tfrac{1}{m}u\Big) + \tfrac{\partial q_{mv}}{\partial t} - \tfrac{\partial q_{av}}{\partial t}\Big)
\end{aligned}
$$

The system has a relative degree r which is smaller than the degree of the system n. $n - r$ state variables are rendered unobservable by state feedback. This is called the zero dynamics of the system, also called internal dynamics. It is that part of the dynamics of the system that cannot be affected by the designed controller. A stability condition for this system lies in the fact that this zero dynamics must have asymptotically minimum phase, i.e, the state variables are automatically converging to an attractor or solution.
In order to design a controller the system can be transformed into the normal form using the coordinate transformation $(z_1, z_2, v_1, \ldots, v_{n-r}) = (h(p), L_f h(p), \eta_{r+1}, \ldots, \eta_n)$. The functions $\eta_{r+1} \ldots \eta_n$ are arbitrary chosen functions of the states such that:

$$
\frac{\partial}{\partial p}\begin{bmatrix} h(p) \\ L_f h(p) \\ \eta_{r+1} \\ . \\ . \\ \eta_n \end{bmatrix}
$$

is invertible to establish n linearly independent vector fields. The following system in the canonical form appears:

$$\dot{z_1} = z_2 \tag{C.2}$$

$$\dot{z_2} = \Big(\frac{1}{(\rho l_{mv} + L_{ven}A_{mv})C_p}\Big)\Big((v_4 - z_1)A_{mv} - \frac{\rho v_2^2}{2A_{mv}}\Big)$$

$$-\Big(\frac{1}{(\rho l_{av} + L_{art}A_{av})C_p}\Big)\Big((z_1 - v_5)A_{av} - \frac{\rho v_3^2}{2A_{av}}\Big)$$

$$-\frac{d}{mC_p}\Big(C_p z_2 - v_2 + v_3\Big) + \frac{A_z}{mC_p}u \tag{C.3}$$

$$\dot{v} = \zeta(z, v, t) \tag{C.4}$$

A stabilizing controller for this system with the assumption that the zero dynamics is asymptotically minimum phase, has the form:

$$u = \frac{mC_p}{A_z}\Bigg(- \Big(\frac{1}{(\rho l_{mv} + L_{ven}A_{mv})C_p}\Big)\Big((v_4 - z_1)A_{mv} - \frac{\rho v_2^2}{2A_{mv}}\Big)$$

$$+\Big(\frac{1}{(\rho l_{av} + L_{art}A_{av})C_p}\Big)\Big((z_1 - v_5)A_{av} - \frac{\rho v_3^2}{2A_{av}}\Big)\Bigg)$$

$$+\frac{mC_p}{A_z}\Bigg(\frac{d}{mC_p}\Big(C_p z_2 - v_2 + v_3\Big) + K_1(p_{lv} - z_1) - K_2 z_2\Bigg) \tag{C.5}$$

where K_1 and K_2 are chosen such that the polynomial $\lambda^2 + K_2\lambda + K_1 = 0$ is Hurwitz, i.e. has all its poles in the left half complex plane.
The connection between the piston position x_1 and the desired pressure p_{lv} is formed by the time-varying elastance model $E(t)$. The relation between desired pressure and position of the piston becomes:

$$p_{lv} = E(t)(A_z(L_0 - x_1) - V_0) \tag{C.6}$$

The stability of the complete system, i.e., the stability of the remaining zero dynamics is shown making use of a stabilization method applied to nonlinear systems with a periodic solution. It shows a marginally stable closed loop system. In appendix D this method is explained in detail.
Unfortunately, the strategy described above has a stabilizing controller (C.5) that is rather difficult to implement. A lot of uncertain parameters are supposed to be known. Furthermore, the measured pressure signal used in the feedback loop has been superimposed

with noise due to measurement noise in the pressure sensor and uncorrelated high frequent noise in the servo drive system. The effect of measurement noise on the closed loop output is shown in appendix G.5. It shows the need for good, low-noise sensors.

D Stability analysis

In this section the stability of the complete system is discussed. The closed loop system is nonlinear due to the terms that describe the valve behavior in the system. It is time periodically i.e., in the stationary situation each heartbeat, identical pressures and flows will appear. Furthermore, this system depends explicitly on time by means of the elastance function $E(t)$. Concluding, the closed loop system is a nonlinear non-autonomous time-varying periodic system.
Suppose in this system that $x^p(t) = x^p(t+T)$ is the periodic solution with period time T. The nonlinear system, called here $\dot{x} = f(t, x(t))$, can be linearized around the periodic solution of this system $x^p(t)$, which leads to a linear time-varying system (LTV). The monodromy matrix Φ_T can, for a periodic LTV system, give information on the stability of the equilibrium point of this system (Leine and van de Wouw (2002), Parker and Chua (1989)). In this matrix the fundamental solutions of the periodic system are stored.
The stability of the closed loop system is determined by its characteristic multipliers, also called Floquet multipliers i.e., eigenvalues of the monodromy matrix Φ_T. The Floquet multipliers determine the exponential growth or decay of perturbations in the eigendirections of the monodromy matrix Φ_T and hence the stability of the periodic solution. If a Floquet multiplier has a magnitude larger (smaller) than one, a perturbation of the initial condition in the corresponding eigendirection will grow (decay) after one period of oscillation.
The monodromy matrix $\Phi_T = \Phi(T + t_0, t_0)$ maps an initial condition $\Delta x(t_0)$ to the response $\Delta x(T + t_0)$ at time $T + t_0$, one period later. The matrix $\Phi(t)$ is called the fundamental solution matrix. In this matrix a set of the nine independent, fundamental solutions $\phi_1(t,), ..., \phi_9(t)$ of the system are stored. The linearized LTV system has the form:

$$\dot{x}(t) = A(t)x(t) \tag{D.1}$$

with $A(t)$ time-dependent. The perturbation equation excluding the higher order terms becomes then:

$$\Delta\dot{x}(t) = A(t)\Delta x(t) \tag{D.2}$$

Considering $\Delta x(t)$ in (D.2) to be a perturbation around a trajectory of the nonlinear non autonomous time-varying periodic system. The fundamental solution matrix relates how an infinitely small perturbation evolves to an infinitely small perturbation after a period time T (figure D.1). A solution of the initial value problem starting at $x^p(t_0)$ evolves during a time $t_d = T + t_0$ to $x^p(T + t_0)$. If the initial condition is perturbed with a small

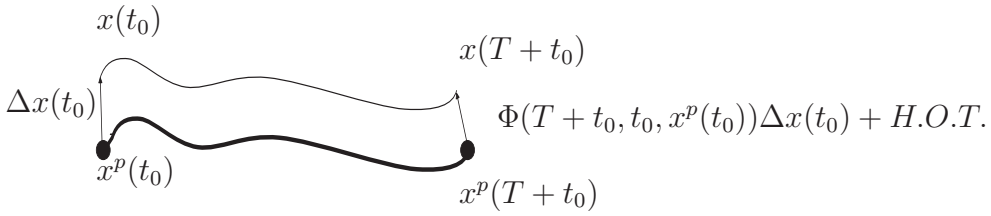

Figure D.1: *Definition of the fundamental solution matrix.*

perturbation $\Delta x(t_0) = x(t_0) - x^p(t_0)$, the perturbed solution will evolve during a time t_d to $x(T + t_0)$. The perturbation on the initial condition $\Delta x(t_0)$ yields a perturbation $\Delta x(T + t_0) = x(T + t_0) - x^p(T + t_0)$ after a period time T. The monodromy matrix relates $\Delta x(t_0)$ to $\Delta x(T + t_0)$ as:

$$\Delta x(T + t_0) = \Phi(T + t_0, t_0, x^p(t_0))\Delta x(t_0) + H.O.T. \tag{D.3}$$

It should be noted that the higher-order terms vanish when infinitely small perturbations are considered. The fundamental solution matrix can now be obtained by solving the following initial value problem:

$$\dot{\Phi}(T + t_0, t_0, x^p(t_0)) = \frac{\partial f(x,t)}{\partial x} \mid_{x^p(t)} \Phi(T + t_0, t_0, x^p(t_0)), \tag{D.4}$$

$$\Phi(t_0, t_0, x^p(t_0)) = I.$$

Unfortunately, in general it is not possible to give an analytical solution for (D.4) because it is a LTV system. For LTV systems the fundamental solution matrix cannot be written as an exponential function of the system matrix $\frac{\partial f(x,t)}{\partial x} \mid_{x^p(t)}$ as can be done for linear time invariant systems. Therefore, solutions of (D.4) should in general be calculated by numerical integration, taking the appropriate initial conditions into account. The single shooting method finds periodic solutions of a system by solving a two-point boundary value problem, in which solutions are sought of $H(x_0, T) \equiv x_T - x_0 = 0$. H represents the nonlinear system $f(x, t)$. T is the period time of the periodic solution and x_0 is a state on the periodic solution. The zero of this function is found by the Newton-Raphson method (D.5).

$$\frac{\partial H}{\partial x_0}\Delta x_0 + \frac{\partial H}{\partial T}\Delta T_0 = x_0 - x_T \tag{D.5}$$

After evaluation of the partial derivatives of this function and addition of an anchor equation to create a solution for the system, the following set of equations appear that have to be solved (Leine and van de Wouw (2002)):.

$$\begin{bmatrix} \Phi_T(x_0^{(i)}) - I & f(x_T^{(i)}) \\ f(x_0^{(i)})^T & 0 \end{bmatrix} \begin{bmatrix} \Delta x_0^{(i)} \\ \Delta T^{(i)} \end{bmatrix} = \begin{bmatrix} x_0^{(i)} - x_T^{(i)} \\ 0 \end{bmatrix} \tag{D.6}$$

The anchor equation is used because (D.5) is a system with n equations in $n+1$ unknowns (the n components of x_0 and period T). The shooting method solves in each iteration step the set of equations D.6 and then updates

$$\begin{bmatrix} x_0^{(i+1)} \\ T^{(i+1)} \end{bmatrix} = \begin{bmatrix} x_0^{(i)} \\ T^{(i)} \end{bmatrix} + \begin{bmatrix} \Delta x_0^{(i)} \\ \Delta T^{(i)} \end{bmatrix} \tag{D.7}$$

with initial guesses $x_0^{(0)}$ and $T^{(0)}$. The subscripts have been added to indicate the iteration count. This scheme is reiterated until some convergence criterion is met.

D.1 Stability of concept with feedback of piston position x_1

The stability of the complete system has been determined by solving the monodromy matrix Φ_T and determine the eigenvalues of this matrix. The characteristic multipliers, or Floquet multipliers belonging to this monodromy matrix are:
$\lambda_1 = 0.50$
$\lambda_2 = -0.29$
$\lambda_3 = -0.38 \cdot 10^{-1}$
$\lambda_4 = 0.81 \cdot 10^{-2}$
$\lambda_5 = -0.43 \cdot 10^{-2}$
$\lambda_6 = -0.31 \cdot 10^{-5}$
$\lambda_7 = 1$
$\lambda_8 = 1$
$\lambda_9 = 1$
The Floquet multipliers are all within the unit circle, except for three. Those Floquet multipliers are on the unit circle. From Parker and Chua (1989) it is said that, then the periodic solution is on the verge of instability (marginally stable). This means that if a disturbance is applied to the system in the direction of the eigenvector belonging to the Floquet multiplier with value 1, then the applied disturbance will not vanish nor explode but stays on the periodic solution. To show this effect, a disturbance ϵ is applied to the system in the direction of one of the eigenvectors with Floquet multiplier 1. The numerical results of a disturbance with a normally distributed random number around zero and a variance of 0.01 applied to the system, are shown in figure D.2. From these figures, it can be concluded that all nine states are not diverging from the periodic solution.

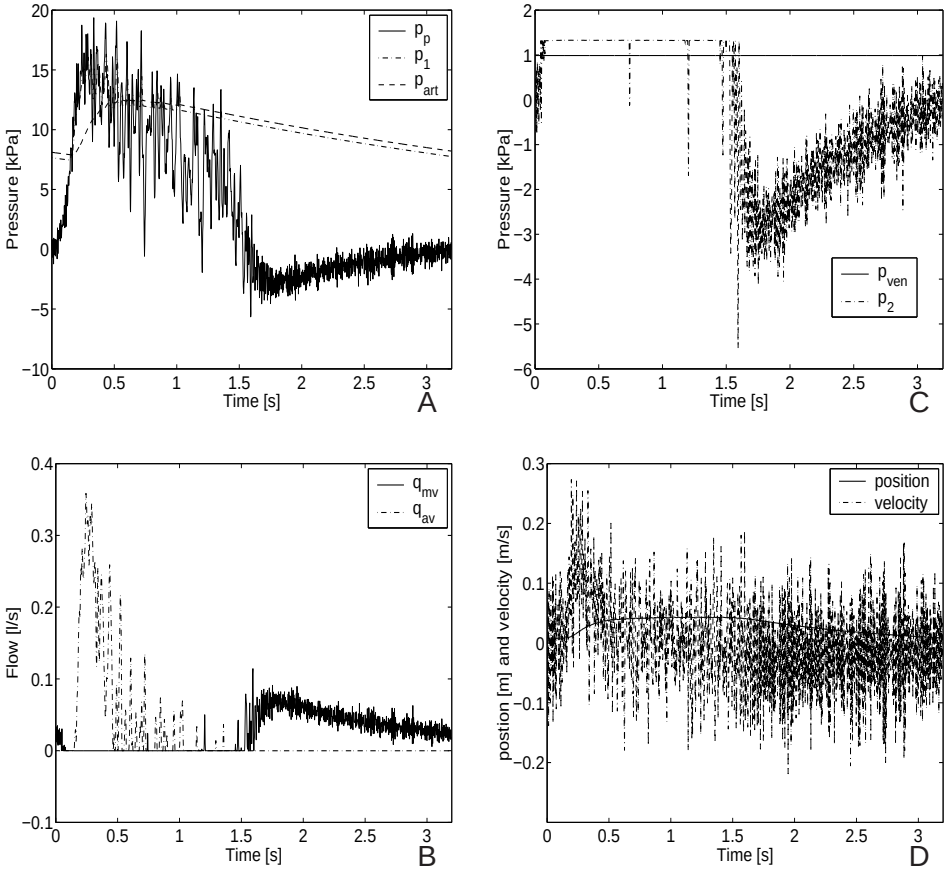

Figure D.2: ***A****: Pump pressure, pressure proximal p_1 to the RC parallel connection and arterial pressure simulated with a disturbance in the eigendirection of $\lambda = 1$.* ***B****: Aortic flow q_{av} and mitral flow q_{mv} as a function of time after application of the disturbance.* ***C****: Venous and pressure proximal p_2 to the RC parallel connection.* ***D****: The position x_1 and velocity x_2 of the piston.*

D.2 Stability of concept with feedback of pump pressure p_p

The stability of the closed loop system for this concept (C) is also determined by solving the monodromy matrix Φ_T and calculate the eigenvalues of this matrix. It becomes clear whether or not the zero dynamics of the closed loop system is internally stable. The characteristic multipliers, or Floquet multipliers belonging to this monodromy matrix are:
$\lambda_1 = 0.54$
$\lambda_2 = -0.19 \cdot 10^{-2}$
$\lambda_3 = -0.17 \cdot 10^{-2}$
$\lambda_4 = 0.12 \cdot 10^{-3}$
$\lambda_5 = -0.45 \cdot 10^{-5}$
$\lambda_6 = -0.12 \cdot 10^{-5}$
$\lambda_7 = 1$
$\lambda_8 = 1$

$\lambda_9 = 1$
Also here the system is on the verge of instability due to the Floquet multipliers with value 1.

E FRF and servo controller design for the heart valve tester

In the linear control theory the most common method for an indication of the system behavior is the frequency response design method. Frequency response design is popular primarily because it provides good designs in the face of uncertainty in the plant model. For example, for systems with poorly known or changing high-frequency resonances, their feedback compensation can be tempered to alleviate the effects of those uncertainties. Another advantage of using frequency response design method is the ease with which experimental information can be used for design purposes. Raw measurements of the output amplitude and phase of a plant undergoing an excitation that includes all frequencies in a certain specified area are sufficient to design a suitable feedback control. However, it is still important to analyze this method critically. In appendix F is shown how to handle and work with frequency response functions.
The FRF measurement of the heart valve tester has been determined using the sensitivity method (figure E.1, panel **A**). The coherence of the sensitivity is plotted for a good measurement quality indication (figure E.1, panel **B**). For low frequencies the coherence is bad. This is due to the uncertain nonlinearities such as coulomb and viscous friction. For higher frequencies the coherence has the tendency to go to one, which means a good measurement. The bode diagram in the left panel of this figure shows for high frequencies noise. This can be contributed to the fact that the magnitude is fluctuating between its encoder accuracy due to analog to digital conversion. Another reason for this high frequency noise is the fact that the sensitivity approaches one for high frequencies (F.12). Thus, the transfer function estimation approaches zero in this area. A little disturbance in the sensitivity measurement, causes relative large fluctuations in the transfer function estimation.
In appendix G a brief introduction about the dynamics used for controller design is given (Franklin et al. (1996) and Bosgra et al. (2003)). For the heart valve tester a controller has to be designed such that a third order reference trajectory is followed with a final maximum overshoot of 10% of the setpoint and a final value accuracy of 10 μm preserving stability and robustness quantities. The maxima of the jerk, acceleration and velocity of the trajectory are respectively 100000 *rad/*s^3, 800 *rad/*s^2 and 90 *rad/s*.
For the controller a lead and lag filter in combination with an integral action is used. The integral action (E.1) takes care of the disturbance rejection and thus lowering the sensitivity function in the low frequency area.

$$C_{int}(s) = \frac{s + 2\pi f_i}{s} \tag{E.1}$$

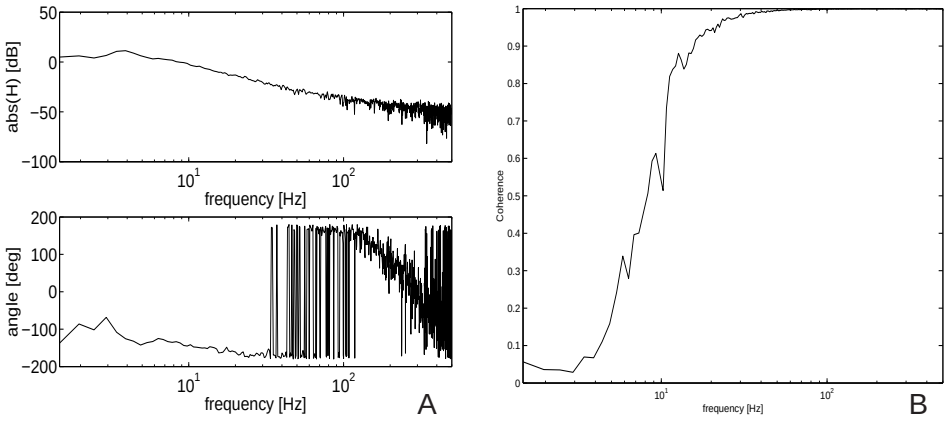

Figure E.1: ***A****: Frequency response measurement of the valve tester.* ***B****: Coherence function for the FRF measurement.*

Making the loop gain large at low frequencies may result in a Nyquist plot that shows unstable behavior. Even if the closed loop system is stable, the gain and phase margins may be unacceptably small, resulting in nearly unstable behavior. To obtain the required phase advance in the resonance frequency region, a lead filter is implemented (E.2). The lead filter takes care of the specified frequency domain quantities to guarantee stability and robustness.

$$C_{lead}(s) = K_l \frac{\frac{1}{2\pi f_1}s + 1}{\frac{1}{2\pi f_2}s + 1} \tag{E.2}$$

with $f_1 < f_2$. Phase lead compensation increases the bandwidth and, hence, makes the closed loop system faster. Keeping the Nyquist plot away from the critical point -1 has the effect of improving the transient response.
For measurement noise reduction and high frequency robustness high frequency roll-off compensation is introduced. This is included by additional lag compensation (E.3).

$$C_{rolloff}(s) = \frac{1}{\frac{1}{(2\pi f_r)^2}s^2 + \frac{1}{2\pi f_r} + 1} \tag{E.3}$$

Discretization of these filters making them applicable for real time application is done using Tustin's Method in combination with prewarping (Shahian and Hassul (1993)). This method converts analog filters to equivalent digital filters. A description of this method is shown in appendix H.
The controller transfer function of the feedback part is shown in panel **A** of figure E.2. In panel **B** is the open loop system plotted with a bandwidth of $30\,Hz$ and a phase advance of $45°$. In panel **C** the sensitivity function is shown. Panel **D** shows the Nyquist plot of the open loop gain. Stability and robustness are preserved within the frequency domain specifications (section G.8).
The tracked and reference trajectory is presented in panel **E** of figure E.2. Panel **F** shows the error belonging to this trajectory. The output is within specifications. Application of

a typical reference trajectory for the control scheme (figure E.3, panel **A**) shows error margins smaller than 0.3 *mm* (panel **B**).

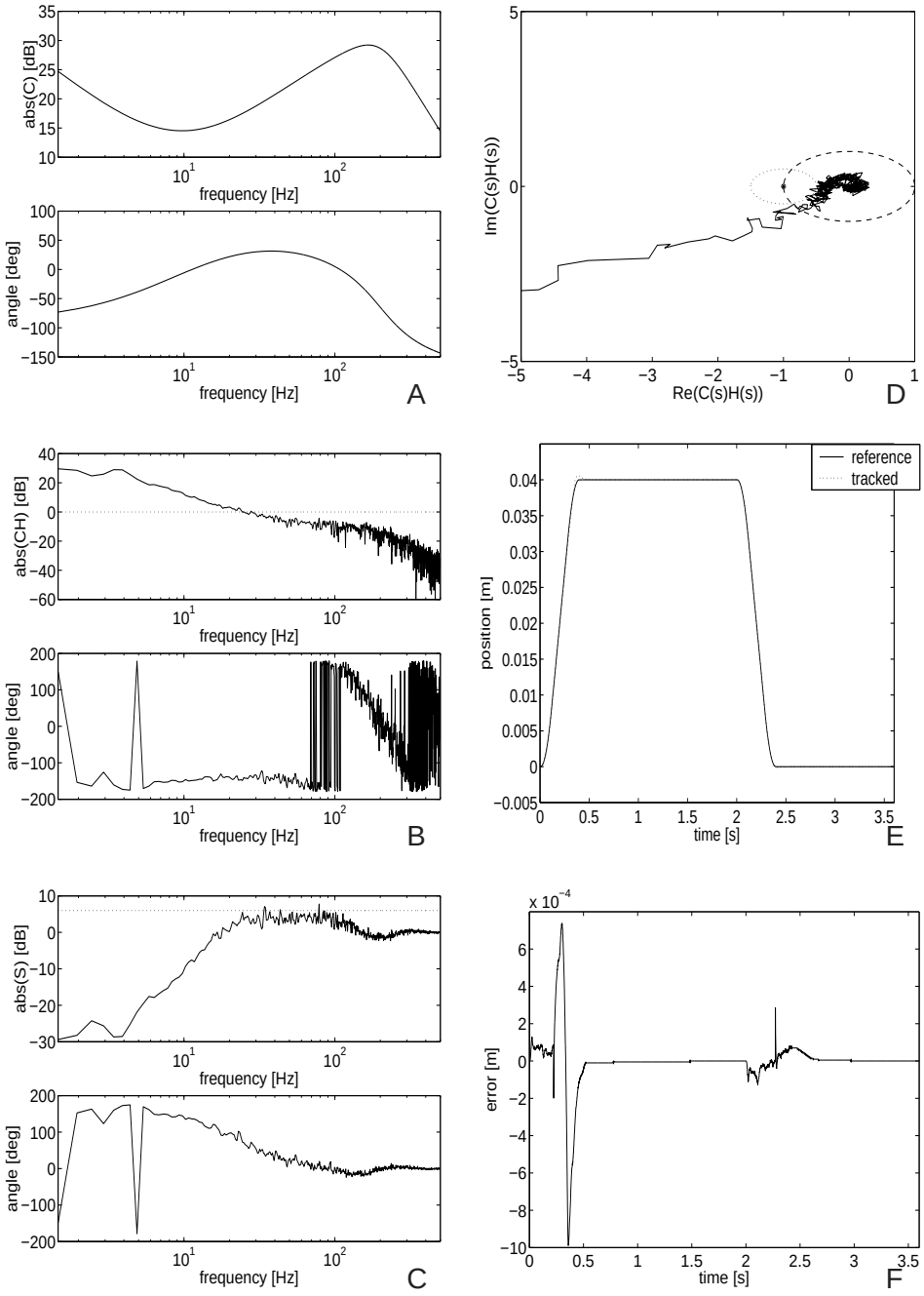

Figure E.2: ***A**: Frequency response of the controller for the valve tester. **B**: Open loop frequency response. **C**: Frequency response of the sensitivity function. **D**: Nyquist plot of the open loop response. **E**: Tracked trajectory and reference signal. **F**: Error signal of tracked trajectory.*

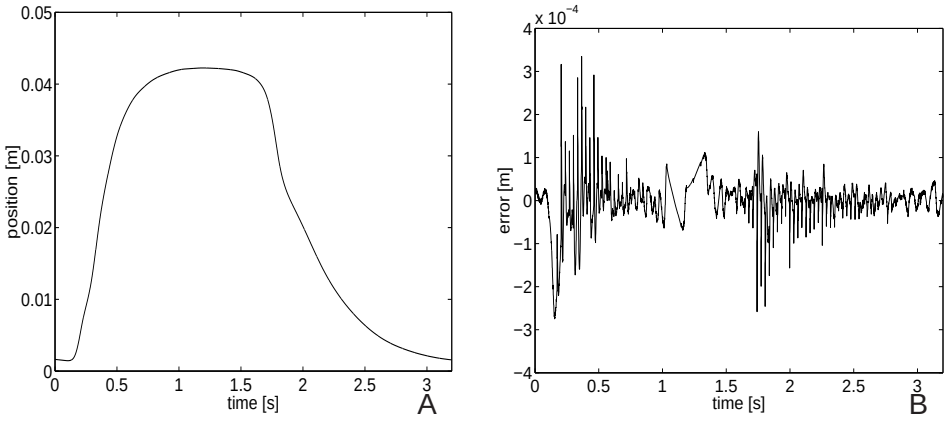

Figure E.3: ***A****: Reference position signal after activation of the control algorithm.* ***B****: Error signal between reference and tracked position signal after activation of the control algorithm.*

F Measuring frequency response functions

The most common way to perform a frequency response function (FRF) measurement is to make use of cross- and autopowerspectra. In the open loop case the measured crosspowerspectrum is divided by the measured autopowerspectrum to create an estimator for the frequency response function. The use of these spectra takes care that uncorrelated extraneous noise does not disturb the estimated frequency response function. In a closed-loop environment, it is no longer usual to look at the input and the output. Then the use of spectra to determine a FRF measurement, gives a biased result in the case of extraneous noise (Boot et al. (2003)).

In figure F.1 a linear system in closed loop is shown. The input $r(t)$ describes a reference

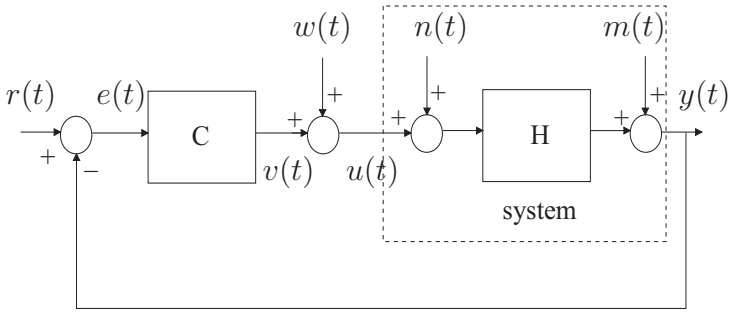

Figure F.1: *Block diagram of a closed loop system.The input $r(t)$ is a reference trajectory. $e(t)$ is the error. Both $n(t)$ and $m(t)$ are random uncorrelated noises. $w(t)$ is an extra input used for system excitation. $u(t)$ and $y(t)$ are the system in- and output, respectively.*

trajectory. Both $n(t)$ and $m(t)$ are random uncorrelated noises which can be influenced by any input. For the analysis the system needs to be excitated. Therefore an extra input $w(t)$ is used. From the analysis in Boot et al. (2003) the direct method and the sensitivity method are chosen to compare with each other. What follows is a short overview of that

analysis. A handy tool used in this analysis is the fact that the spectral density function can be found via fourier transforms. In (F.1) the cross correlation is shown.

$$S_{uy}(f) = \lim_{T\to\infty} \frac{1}{T} U^*(f)Y(f) \tag{F.1}$$

where U^* is the complex conjugated of U and T is the total sample time. From now on large time samples are assumed and the limit sign is left behind. Furthermore, it is assumed that the inputs are independent, so the correlations and spectra between them are zero, $S_{rw} = S_{rn} = S_{rm} = S_{wn} = \ldots = 0$. Writing the system equations for the different points in the loop:

$$\begin{aligned}
U(f) &= S(f)C(f)R(f) + S(f)W(f) - S(f)C(f)H(f)N(f) - S(f)C(f)M(f) \\
Y(f) &= S(f)C(f)H(f)R(f) + S(f)H(f)W(f) + S(f)H(f)N(f) + S(f)M(f) \\
V(f) &= S(f)C(f)R(f) - S(f)C(f)H(f)W(f) - S(f)C(f)H(f)N(f) - S(f)C(f)M(f) \\
E(f) &= S(f)R(f) - S(f)H(f)W(f) - S(f)H(f)N(f) - S(f)M(f)
\end{aligned} \tag{F.2}$$

where

$$S(f) = \frac{1}{1 + C(f)H(f)} \tag{F.3}$$

F.1 Direct method

The direct method is the direct measurement of the system. The output $y(t)$ of the system will be divided by the input $u(t)$. An estimation of the transfer function will be:

$$\hat{H} = \frac{S_{uy}}{S_{uu}} \tag{F.4}$$

The spectral density functions and the transfer function estimation are, respectively

$$\begin{aligned}
S_{uy} &= \frac{1}{T} U \cdot Y \\
&= \frac{1}{T}\Big((S \cdot SC \cdot CH)S_{rr} + (S \cdot SH)S_{ww} - (S \cdot SC \cdot H \cdot H)S_{nn} - (S \cdot SC)S_{mm} \Big)
\end{aligned}$$

(F.5)

$$S_{uu} = \frac{1}{T} U \cdot U$$

$$= \frac{1}{T}\Big((S \cdot SC \cdot C)S_{rr} + (S \cdot S)S_{ww} + (S \cdot SC \cdot CH \cdot H)S_{nn} + (S \cdot SC \cdot C)S_{mm}\Big)$$

(F.6)

$$\hat{H} = \frac{(C \cdot CH)S_{rr} + H \cdot S_{ww} - (C \cdot H \cdot H)S_{nn} - C \cdot S_{mm}}{(C \cdot C)S_{rr} + S_{ww} + (C \cdot CH \cdot H)S_{nn} + (C \cdot C)S_{mm}} \tag{F.7}$$

From this equation it is concluded that at the moment the signal S_{ww} is only present, the frequency response function $H(f)$ is measured. However, when there is extraneous noise this takes care for a biased estimate of the FRF. In the extreme situation with only noise $-\frac{1}{C}$ will be measured.
Furthermore, the coherence function is a good indication whether a measured frequency response function is reliable or not. A good FRF is measured if the coherence tends to go to 1 in the whole frequency range. It is defined as follows:

$$\gamma^2_{uy}(f) = \frac{|S_{uy}(f)|^2}{S_{uu}(f)S_{yy}(f)} \tag{F.8}$$

Writing out the whole coherence function for this case becomes very large and inconvenient. For the illustration only the terms $w(t)$ and $n(t)$ are taken along.

$$\gamma^2_{uy}(f) \approx \frac{|H|^2|S|^4S^2_{ww} - 2|C||H|^3|S|^4S_{ww}S_{nn} + |C|^2|H|^4|S|^4S^2_{nn}}{|H|^2|S|^4S^2_{ww} + 2|C|^2|H|^4|S|^4S_{ww}S_{nn} + |C|^2|H|^4|S|^4S^2_{nn}} \tag{F.9}$$

Using the direct method it can be concluded that undesired noise causes a distortion in the estimated FRF. The coherence function does not give much grip too because in the case of only extraneous noise it will also go to one.

F.2 Sensitivity method

The sensitivity method is the most common technique for FRF measurements in closed loop. This method measures the input to the system $u(t)$ and the excited extra input $w(t)$ to determine an estimation of the sensitivity function $\hat{S}$, and thus the transfer function $\hat{H}$.

$$S_{wu} = \frac{1}{T} W \cdot U = S \cdot S_{ww} \tag{F.10}$$

$$\hat{S} = \frac{S_{wu}}{S_{ww}} = S \tag{F.11}$$

The advantage can directly be seen. When measuring the sensitivity, there will be no bias. The transfer function $H(f)$ will be now:

$$H(f) = \frac{1 - S(f)}{C(f)S(f)} \tag{F.12}$$

With this method the coherence function will be:

$$\gamma^2_{wu}(f) = \frac{S_{ww}}{|C|^2 S_{rr} + S_{ww} + |C|^2|H|^2 S_{nn} + |C|^2 S_{mm}} \tag{F.13}$$

The advantage of measuring the sensitivity is that undesired uncorrelated noise averages itself out (F.11). Also the coherence function will become lower with more uncorrelated noise from outside, which makes it a good measurement quality indicator.

G Introduction to controller design

A closed loop model scheme is shown in figure G.1. By solving the signal balance

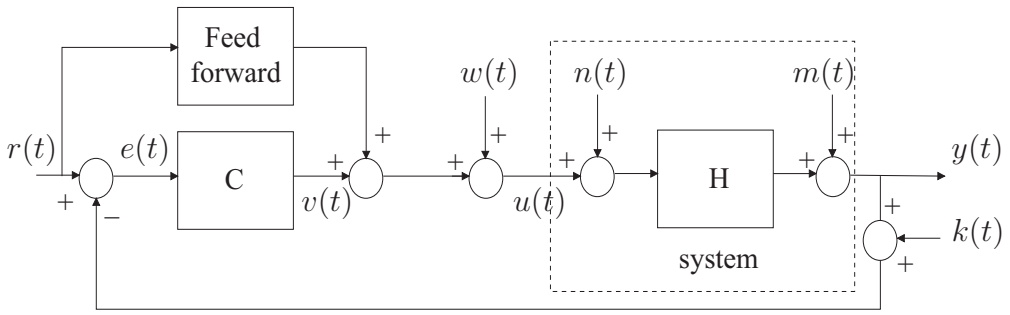

Figure G.1: *Block diagram of a closed loop system.The input $r(t)$ is a reference trajectory. $e(t)$ is the error. Both $n(t)$ and $m(t)$ are random uncorrelated noises. $w(t)$ is an extra input used for system excitation. $u(t)$ and $y(t)$ are the system in- and output, respectively. $k(t)$ is the input for measurement noise.*

$y(s) = m(s) + H(s)\Big(w(s) + C(s)r(s) - C(s)y(s) - C(s)k(s) + n(s)\Big)$ for the output

$y(s)$, it can be shown that:

$$y(s) = \frac{1}{1 + C(s)H(s)} m(s) + \frac{C(s)H(s)}{1 + C(s)H(s)} (r(s) - k(s)) + \frac{H(s)}{1 + C(s)H(s)} (n(s) + w(s)) \tag{G.1}$$

G.1 Closed loop stability

The open loop transfer function CH plotted in the complex plane is called a Nyquist plot. This plot is useful in determine stability, passing side of the point -1, and robustness, distance to the point -1. The Nyquist stability criterium relates the open loop frequency response to the number of closed loop poles of the system in the right half plane. Looking at the closed loop transfer function (G.2),

$$H_{cl} = \frac{y(s)}{r(s)} = \frac{C(s)H(s)}{1 + C(s)H(s)} \tag{G.2}$$

The closed loop roots are the solutions of $1 + C(s)H(s) = 0$. For stability, no closed loop poles are allowed in the right half plane. From Franklin et al. (1996), the argument principle has the following essence:

> 'A contour map of a complex function will only encircle the origin if the contour contains a singularity, pole or zero, of the function.'

The principle can be extended by allowing multiple singularities within the contour. The number and direction of origin encirclements then change. To apply this principle to control design, it is supposed the contour in the s-plane encircles the entire right half plane. If the evaluation contour of s enclosing the right half plane contains a pole or zero of $1 + C(s)H(s) = 0$, then the evaluated contour of $1 + C(s)H(s)$ will encircle the origin. Notice that $1 + C(s)H(s)$ is simply $C(s)H(s)$ shifted to the right 1 unit and $C(s)H(s)$ can be plotted. That is the reason why -1 is the critical point in a Nyquist plot.

G.2 Disturbance rejection and bandwidth

To study disturbance rejection, consider the block diagram of figure G.1, where $m(t)$ represents the equivalent disturbance at the output of the plant. This transfer function is called the sensitivity function of the closed loop system (G.3).

$$S(s) = \frac{y(s)}{m(s)} = \frac{1}{1 + C(s)H(s)} \tag{G.3}$$

The smaller $|S(j\omega)|$ is, the more the disturbances are rejected at the angular frequency ω. $|S|$ is small if the magnitude of the loop gain CH is large. Hence, for disturbance attenuation it is necessary to shape the loop gain such that it is large over those frequencies where disturbance attenuation is needed.
Making the loop gain CH large over a large frequency band easily results in error signals and resulting plant inputs u that are larger than the plant can absorb. Therefore, CH can only be made large over a limited frequency band. This is usually a low pass band or integral action, that is, a band that ranges from frequency zero up to the bandwidth of the feedback loop. The larger the 'capacity' of the plant is, the larger the inputs are the plant can handle before it saturates or otherwise fails, the larger the maximally achievable bandwidth usually is.

G.3 Command response

The response $y(s)$ to the command signal $r(s)$ is shown in (G.1) and (G.2). This is called the complementary sensitivity function T. Adequate loop shaping ideally results in a complementary sensitivity function T that is close to 1 up to the bandwidth, and transits smoothly to zero above this frequency. The closed loop transfer function ideally is low pass with the same bandwidth as the frequency band for disturbance rejection.

G.4 Plant capacity

Any physical plant that has limited 'capacity', can absorb inputs of limited magnitude only. Looking at the block diagram of figure G.1, the signal balance $u(s) = w(s) + C(s)\Big(r(s) - k(s) - m(s) - H(s)n(s) - H(s)u(s)\Big)$. This may be solved for u (G.4).

$$u = \frac{1}{1 + C(s)H(s)}w(s) + \frac{C(s)}{1 + C(s)H(s)}\Big(r(s) - k(s) - m(s) - H(s)n(s)\Big) \tag{G.4}$$

This function determines the sensitivity of the plant input to disturbances and the command signal. It is known as the input sensitivity function $M = \frac{C(s)}{1+C(s)H(s)}$. If the loop gain CH is large then the input sensitivity M approximately equals the inverse of the plant transfer function. If the open loop plant has zeros in the right half plane then $\frac{1}{H}$ is unstable. Because of this the right half plane open loop plant zeros limit the closed loop bandwidth. To prevent overly large inputs, generally M should not be too large.

G.5 Measurement noise

To study the effect of measurement noise on the closed loop output, the response $y(s)$ to the measurement noise $k(s)$ is considered (G.1). This shows that the influence of the measurement noise $k(s)$ on the control system output is determined by the complementary sensitivity function T. For low frequencies, where by the other design requirements T is close to 1, the measurement noise fully affects the output. This emphasizes the need for good, low-noise sensors.

G.6 Stability robustness

For stability robustness it is necessary to keep the Nyquist plot away from the point -1. The target is to achieve satisfactory gain, phase and modulus margins. It is consistent with the other design targets to have the sensitivity S small in the low frequency range, and T small in the complementary high frequency range.
The faster T decreases with frequency, called roll-off, the more protection the closed loop system has against high-frequency loop perturbations. This is important because owing to neglected dynamics, high frequency uncertainty is ever present. Small values of the sensitivity function for low frequencies, which are required for adequate disturbance rejection, ensure protection against perturbations at low frequencies. Such perturbations are often caused by load variations, friction and cogging effects. In the crossover region neither S nor T can be small. This is the region where the loop gain CH crosses the value 1, the zero *dB* line. It is the region that is most critical for robustness. Peaking of S and T in this frequency region is to be avoided. Good gain, phase and modulus margins are needed to ensure this.

G.7 Performance robustness

Feedback system performance is determined by the sensitivity function S, the complementary sensitivity function T and the input sensitivity function M (G.5).

$$S = \frac{1}{1 + C(s)H(s)}, \quad T = \frac{C(s)H(s)}{1 + C(s)H(s)} \quad M = \frac{C(s)}{1 + C(s)H(s)} \tag{G.5}$$

Considering the extent to which each of these functions is affected by plant variations, it is supposed, for simplicity, that the system environment is sufficiently controlled so that the controller C is not subject to perturbation. Under this assumption it is sufficient to study only the effect of perturbations on S and T because variations in M are proportional to those in S. In Bosgra et al. (2003) this effect is shown as denoted below.
Denote by CH_0 the nominal loop gain, that is, the loop gain that is believed to be rep-

resentative and is used in the design calculations. Correspondingly, S_0 and T_0 are the nominal sensitivity function and complementary sensitivity function. It is not difficult to establish that when the loop gain changes from its nominal value CH_0 to its actual value CH the corresponding relative change of the reciprocal of the sensitivity function S may be expressed as in (G.6).

$$\frac{\frac{1}{S} - \frac{1}{S_0}}{\frac{1}{S_0}} = \frac{S_0 - S}{S} = T_0 \frac{CH - CH_0}{CH_0} \tag{G.6}$$

Similarly, the relative change of the reciprocal of the complementary sensitivity function may be written as in (G.7).

$$\frac{\frac{1}{T} - \frac{1}{T_0}}{\frac{1}{T_0}} = \frac{T_0 - T}{T} = S_0 \frac{CH - CH_0}{CH_0} = S_0 \frac{\frac{1}{CH} - \frac{1}{CH_0}}{\frac{1}{CH_0}} \tag{G.7}$$

These relations show that for the sensitivity function S to be robust with respect to changes in the loop gain, it is desired that the nominal complementary sensitivity function T_0 to be small. On the other hand, for the complementary sensitivity function T to be robust, it is desired that the nominal sensitivity function S_0 to be small. These requirements are conflicting, because S_0 and T_0 add up to 1 and therefore cannot simultaneously be small. The solution is to have each small in a different frequency range. As seen before, normal control system design specifications require S_0 to be small at low frequencies. This causes T to be robust at low frequencies, which is precisely the region where its values are significant. Complementary, T_0 is required to be small at high frequencies, causing S to be robust in the high frequency range.

G.8 Design goals and criteria

The basic requirements in Franklin et al. (1996) and Bosgra et al. (2003) for a well-designed control system are:

- The transient response is sufficiently fast.
- The transient response shows satisfactory damping.
- The transient response satisfies accuracy requirements, often expressed in terms of error constants.
- The system is sufficiently insensitive to external disturbances and variations of internal parameters.

These basic requirements can be further specified in terms of both a number of frequency-domain specifications and certain time-domain specifications.
Several important frequency domain quantities are:

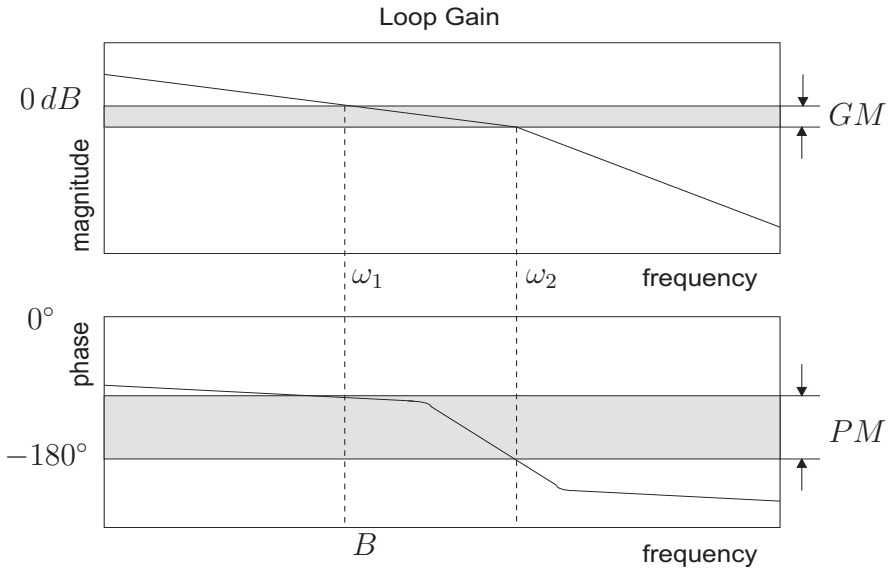

Figure G.2: *Gain and phase margins from the Bode plot of the loop gain CH. GM and PM represents the gain and phase margins, respectively. ω_1 and ω_2 are the frequencies at $0\,dB$ and $180°$, respectively. B represents the bandwidth of the system*

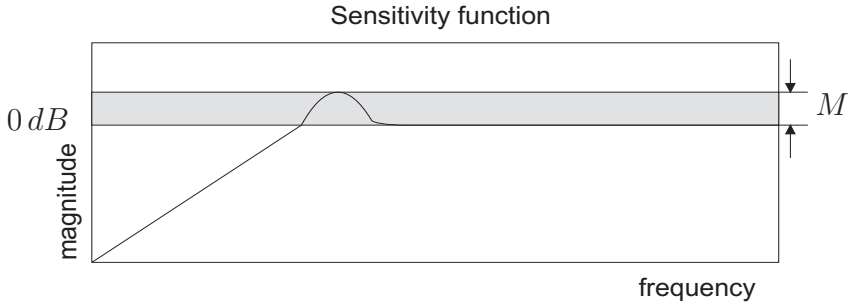

Figure G.3: *Sensitivity plot showing the resonance peak M*

Gain margin. The gain margin measures relative stability. It is defined as the reciprocal of the magnitude of the loop frequency response CH, evaluated at the frequency at which the phase angle is $-180°$. The magnitude of the gain margin must be at least $6\,dB$ at this frequency.

Phase margin. The phase margin also measures relative stability. It is defined as $180°$ plus the phase angle of the loop frequency response CH at the frequency where the gain is unity. The phase margin must be at least $45°$ at the $0\,dB$ crossover frequency.

Bandwidth. The bandwidth measures B measures the speed of response in frequency domain terms. It is defined as the range of frequencies over which the open loop frequency response has a magnitude bigger than $0\,dB$.

Resonance peak. Relative stability may also be measured in terms of the peak value of the magnitude of the closed loop frequency response or sensitivity function, occurring at the resonance frequency. This criterion is included as limiting this resonance frequency to $6\,dB$.

These definitions are illustrated in figures G.2 and G.3. The reference signal in this article is supposed to have a reference trajectory that consists of several different third order set-point trajectories every period. For the controller design a third order reference trajectory $r(t)$ is chosen (figure G.4). This figure shows four important time domain quantities that may be used for performance specifications for the response of the control system output to a third order reference trajectory.

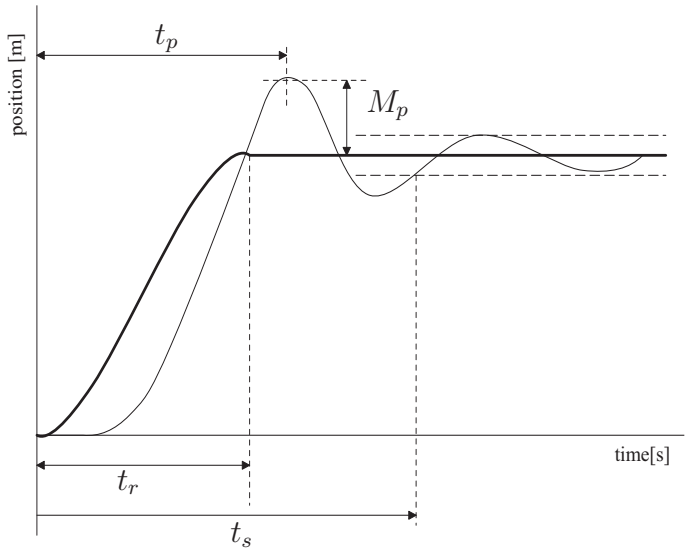

Figure G.4: *Interpretation of a third order reference trajectory. It shows the definition of rise time t_r, settling time t_s, peak time t_p and overshoot M_p.*

Rise time t_r. It is the time it takes the system to reach its new set point.

Settling time t_s. The settling time is defined as the time required for the response to reach and remain within a specified error band of its final value.

Peak time t_p. The peak time is the time it takes the system to reach the maximum overshoot point.

Maximum overshoot M_p. The maximum overshoot is the maximum difference between the transient and the steady-state response.

H Tustin's discretization and prewarping method

Tustin's discretization technique makes use of trapezoidal integration, that is, to approximate $e(t)$ by a straight line between two samples (Shahian and Hassul (1993)).

$$u_k = u_{k-1} + \frac{T_s}{2}(e_{k-1} + e_k) \tag{H.1}$$

or taking the z-transform,

$$D(z) = \frac{U(z)}{E(z)} = \frac{\frac{T_s}{2}(z+1)}{z-1} \tag{H.2}$$

Because this is a numerical integration technique, it can be said that,

$$s \equiv \frac{\frac{2}{T_s}(z-1)}{z+1} \Rightarrow z \equiv \frac{1+\frac{T_s}{2}s}{1-\frac{T_s}{2}s} \tag{H.3}$$

The mapping between the s-plane and z-plane is determined by the relationship $z = e^{sT_s}$. It is supposed to be known that the stability region in the s-plane is the entire left half of the plane. Suppose further that a stable pole has the form $-\alpha + j\omega$, then the mapping is:

$$z = e^{(-\alpha+j\omega)T_s} = e^{-\alpha T_s} e^{j\omega T_s} \tag{H.4}$$

Because $e^{-\alpha T_s}$ is the magnitude of z and always smaller than 1 and because ω varies from zero to infinity, a circle with radius 1 or smaller is swept out in the z-plane. This means that the left half of the s-plane maps into the inside of the unit circle in the z-plane.
Let $s = j\omega$ in the Tustin approximation (H.3),

$$z = \frac{1+\frac{T_s}{2}j\omega}{1-\frac{T_s}{2}j\omega} \tag{H.5}$$

From this equation the magnitude and phase are:

$$|z| = \frac{\sqrt{1^2 + (\omega\frac{T_s}{2})^2}}{\sqrt{1^2 + (-\omega\frac{T_s}{2})^2}} = 1 \qquad \phi_z = \frac{\arctan(\frac{\omega T_s}{2})}{-\arctan(\frac{\omega T_s}{2})} = 2\arctan(\frac{\omega T_s}{2}) \tag{H.6}$$

As ω increases, the phase increases while the magnitude stays constant at 1. Thus, a unit circle is swept out. The trapezoidal technique maps the left half plane in the s-plane, into the unit circle in the z-plane (figure H.1). Thus, a stable $D(s)$ results in a stable $D(z)$ using Tustin's approximation.
To prevent frequency distortion, critical frequency prewarping is applied. First, examine the following term in (H.3) for $s = j\omega$:

$$\frac{z-1}{z+1} \rightarrow \frac{e^{j\omega T_s}-1}{e^{j\omega T_s}+1} \tag{H.7}$$

The following relation appears when dividing the numerator and denominator in this equation by $e^{\frac{j\omega T_s}{2}}$.

$$\frac{z-1}{z+1} \rightarrow \frac{2j\sin(\frac{\omega T_s}{2})}{2\cos(\frac{\omega T_s}{2})} = j\tan(\frac{\omega T_s}{2}) \tag{H.8}$$

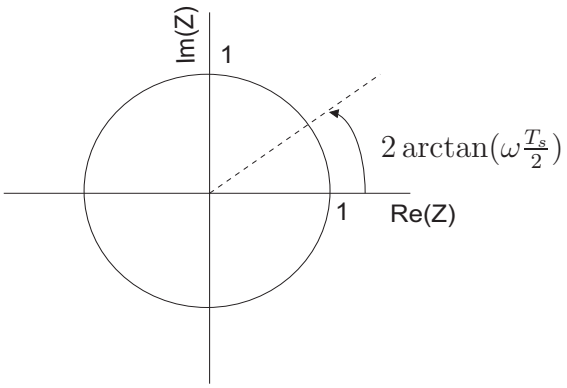

Figure H.1: *Unit circle in the z-domain*

Consider a simple continuous filter with bandwidth a and use Tustin's transformation of this filter.

$$H(s) = \frac{1}{s/a+1} \Rightarrow H(z) = \frac{1}{\frac{2}{T_s}\frac{z-1}{z+1}\frac{1}{a}+1} \tag{H.9}$$

Using (H.8) and let $s = j\omega$, the discrete filter becomes

$$H_z(\omega) = \frac{1}{j\Big(\frac{2}{T_s}\tan(\omega\frac{T_s}{2})\Big)\frac{1}{a}+1} \tag{H.10}$$

The bandwidth of this discrete filter then becomes

$$\omega_{BW} = \frac{2}{T_s}\arctan(\frac{aT_s}{2}) \tag{H.11}$$

This equation gives the relationship between the continuous and discrete equivalent bandwidths. It shows how the frequency scale is distorted by the Tustin transformation. Revisit Tustin approximation by:

$$s \approx K\frac{z-1}{z+1} \tag{H.12}$$

where $K = \frac{2}{T_s}$ in the standard approximation. Try in the following situation to find a K such that at a specific critical frequency $\omega = \omega_c$, the above approximation becomes exact. If

$$K = \frac{\omega_c}{\tan(\frac{\omega_c T_s}{2})} \tag{H.13}$$

is chosen, $H(s)$ and $H(z)$ will be identical at $\omega = \omega_c$. The critical frequency prewarping technique, therefore, becomes:

$$s = \frac{\omega_c}{\tan(\omega_c \frac{T_s}{2})} \frac{z-1}{z+1} \tag{H.14}$$

This equation preserves stability transforming from a stable $D(s)$ to a $D(z)$ and matches the frequency response for breakpoints and for zero frequency. Application of (H.14) to the lead compensator, integral action and frequency roll-off compensator results in the following discrete compensators. For the lead compensator:

$$C_{lead}(z) = \frac{(f_2\alpha + 2\pi f_1 f_2)z - f_2\alpha + 2\pi f_1 f_2}{(f_1\alpha + 2\pi f_1 f_2)z - f_1\alpha + 2\pi f_1 f_2} \tag{H.15}$$

with $\alpha = \frac{f_2}{\tan(f_2 \frac{T_s}{2})}$.
For the integral action:

$$C_{int}(z) = \frac{(\alpha + 2\pi f_i)z - \alpha + 2\pi f_i}{\alpha z - \alpha} \tag{H.16}$$

with $\alpha = \frac{f_i}{\tan(f_i \frac{T_s}{2})}$.
For the frequency roll off compensator:

$$C_{rolloff}(z) = \frac{(2\pi f_r)^2 z^2 + (2\pi f_r)^2 z + (2\pi f_r)^2}{(\alpha^2 + 4\beta\pi f_r \alpha + (2\pi f_r)^2)z^2 + (-2\alpha^2 + 2(2\pi f_r)^2)z + (\alpha^2 + 4\beta\pi f_r \alpha + (2\pi f_r)^2)} \tag{H.17}$$

with $\alpha = \frac{f_r}{\tan(f_r \frac{T_s}{2})}$.

I Experimental and numerical results for three different afterload situations.

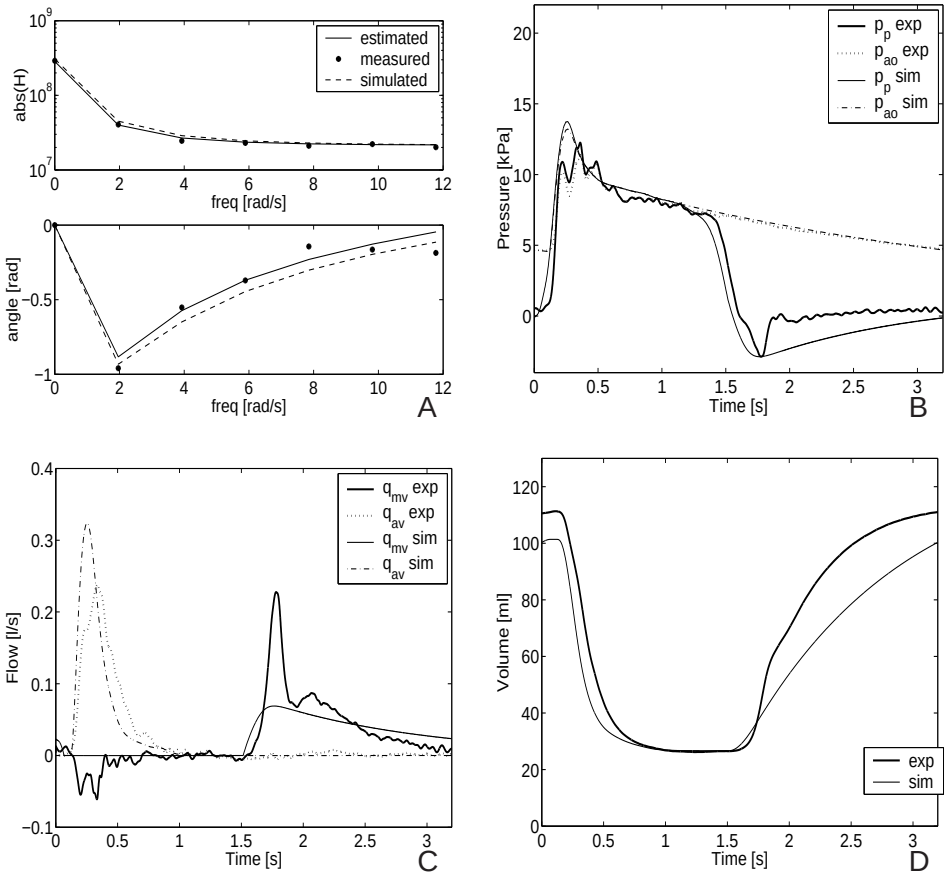

Figure I.1: ***A****: Frequency response function of the afterload impedance Z for the afterload setting marked with exp* 1. ***B****: Numerically(sim) and experimentally(exp) obtained pump pressure p_p and aortic pressure p_{ao} for one cardiac cycle.* ***C****: Aortic q_{ao} and mitral q_{mv} flow.* ***D****: Volume as a function of time calculated by the integration of volume change in aortic and mitral flow.*

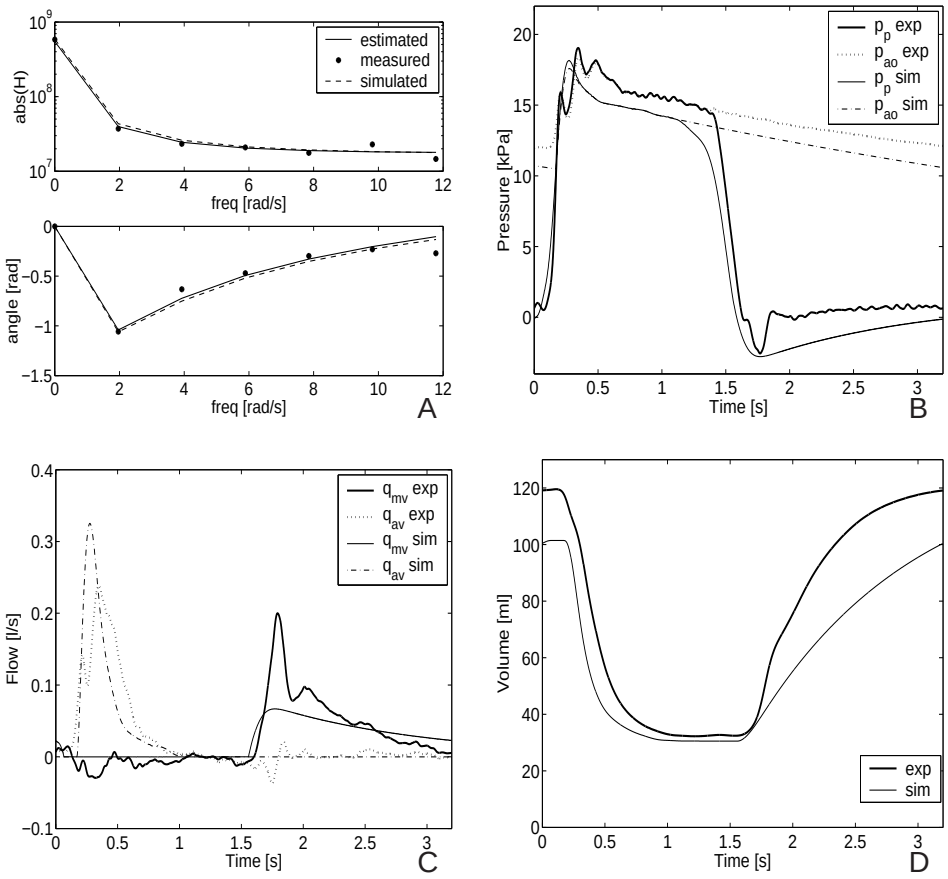

Figure I.2: ***A**: Frequency response function of the afterload impedance Z for the afterload setting marked with exp* 3. ***B**: Numerically(sim) and experimentally(exp) obtained pump pressure p_p and aortic pressure p_{ao} for one cardiac cycle. **C**: Aortic q_{ao} and mitral q_{mv} flow. **D**: Volume as a function of time calculated by the integration of volume change in aortic and mitral flow.*

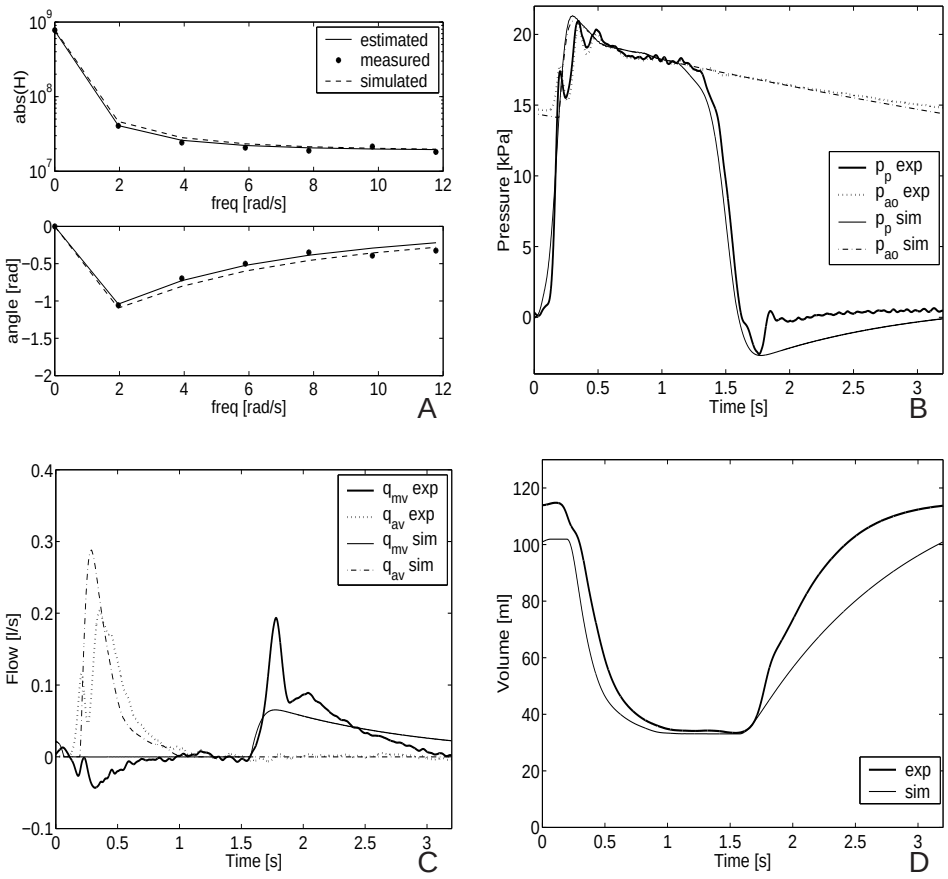

Figure I.3: ***A****: Frequency response function of the afterload impedance Z for the afterload setting marked with exp* 4*.* ***B****: Numerically(sim) and experimentally(exp) obtained pump pressure p_p and aortic pressure p_{ao} for one cardiac cycle.* ***C****: Aortic q_{ao} and mitral q_{mv} flow.* ***D****: Volume as a function of time calculated by the integration of volume change in aortic and mitral flow.*

J List of symbols and subscripts

Symbols			
T_s	s	0.001	sample time
f_i	Hz	7	cut off frequency of integrator compensator
f_r	Hz	300	cut off frequency of roll off compensator
f_1	Hz	13.33	cut off frequency 1 of lead compensator
f_2	Hz	120	cut off frequency 2 of lead compensator
K_l	$-$	3.5	gain of lead compensator
K_1	$-$	1500	control coefficient
K_2	$-$	29.5	control coefficient
q	$m^3 \cdot s^{-1}$	-	flow
x	m	-	state variable
p	Pa	-	pressure
V	m^3	-	volume
R	$Pa \cdot s \cdot m^{-3}$	-	resistance
Z	$Pa \cdot s \cdot m^{-3}$	-	resistance
C	$m^3 \cdot Pa^{-1}$	-	compliance
L	$Pa \cdot s^2 \cdot m^{-3}$	-	inertance
Φ_T	-	-	monodromy matrix
t	s	-	time
t_n	s	-	normalized time
t_d	s	-	perturbation time
t_0	s	-	initial time
t_c	s	-	time since onset of activation
$E(t)$	$Pa \cdot m^{-3}$	-	elastance function
E_n	-	-	normalized elastance function
l	m	-	length of the flow channel
A	m^2	-	valve area

Symbols (continued)

ω	$rad \cdot s^{-1}$	-	continuous frequency
ω_c	$rad \cdot s^{-1}$	-	critical frequency
ω_{BW}	$rad \cdot s^{-1}$	-	bandwidth
α	-	-	real part of a pole
λ	-	-	eigenvalue of monodromy matrix
$e(t)$	m	-	error
$u(t)$	V	-	input
$w(t)$	V	-	external input
$n(t)$	V	-	random uncorrelated noise
$m(t)$	m	-	random uncorrelated noise
$y(t)$	m	-	output
$r(t)$	m	-	reference
$k(t)$	m	-	random uncorrelated measurement noise

Subscripts	
art	arterial
ven	venous
lv	left ventricle
ao	aortic
mv	mitral valve
av	aortic valve
vc	distal to the veins
p	pump
z	piston
des	desired
$filt$	filtered
unf	unfiltered

K Samenvatting

Het nabootsen van het gedrag van het menselijk hart is een belangrijk onderwerp op het gebied van hart fysiologie. Arteriële druk en stroming is een gevolg van de interactie tussen de ventrikel en de arteriële circulatie. Rutten et al. (2005) hebben een bioreactor met een imitatie-circulatie-systeem ontwikkeld om onder andere het functioneren van aortakleppen te testen door het meten van drukken en debieten. Een fysiologische stromingsflux wordt gegenereerd door een voorgeschreven beweging van de zuiger, waarbij de gewenste aortadruk bepaald wordt door tuning van de afsluitimpedantie (afterload). Echter, een nadeel van deze opstelling is dat de stroming door de aortaklep niet wordt bepaald door de klepkarakteristiek. En dit is juist één van de criteria om de kwaliteit van aortakleppen te bepalen. In dit artikel wordt daarom de hartkleppentester van Rutten et al. (2005) uitgebreid met een regelstrategie voor de beweging van de zuiger, om zo de responsie van het hart op veranderingen in klepeigenschappen en afterload, in termen van drukken en debieten, beter na te bootsen.
De regelstrategie is gebaseerd op het tijds-variant elastantie model (Suga and Sagawa (1974)). De elastantieregellus berekent een gewenst pomp volume door het gebruik van de elastantiefunctie en de pompdruk. De volumeregellus regelt het pompvolume om daadwerkelijk een gewenst pomp volume te verkrijgen.
Een mathematisch model van de hartkleppentester is gemaakt om stabiliteit van het toegepaste regelalgoritme te bepalen. Deze wordt bepaald aan de hand van Floquet multipliers (Parker and Chua (1989)). Vervolgens is de regelstrategie geïmplementeerd in de opstelling. Resultaten laten zien dat de regelaar in staat is om te reageren op veranderingen in afterload en klepeigenschappen, waarbij fysiologische drukken en stromingen worden gegenereerd.